DOI: 10.26599/FSHW.2026.9251131

Contents lists available at SciOpen

Food Science and Human Wellness

journal homepage: https://www.sciopen.com/journal/2097-0765

China Food Publishing Co.

Mechanism study on the intervention of type 2 diabetes mellitus by whole bitter melon beverage

Yidan Zhang[1], Yihui Wang[1,2], Xiaoyun Cao[1], Si Huang[1], Taotao Dai[1,2], Lizhen Deng[1,2], Yinong Feng[1,2], Chengmei Liu[1,2], Jun Chen[1,2*]

[1] *State Key Laboratory of Food Science and Technology, Nanchang University, Nanchang, 330047, China*

[2]*International Institute of Food Innovation Co., Ltd., Nanchang University, Jiangxi, China*

ABSTRACT: The hypoglycemic effect of bitter melon and its products has attracted widespread attention. However, the hypoglycemic mechanism of whole bitter melon beverage (WBMB) retaining all nutrients for type 2 diabetes mellitus (T2DM) remains unclear. The results of this study indicated that WBMB improved hyperglycemia, hyperlipidemia, oxidative stress and inflammatory markers levels, alleviated liver and pancreas damage. Moreover, it down-regulated the expression of SRC, STAT3 and PIK3R1, and up-regulated the expression of AKT1 and PIK3CA in T2DM mice in a dose-dependent manner. Simultaneously, the composition and structure of the flora were changed by up-regulating *Bacteroidetes*, *Akkermansia*, *Bifidobacteria,* and down-regulating *Dubosiella* abundance. In addition, the WBMB normalizes serum metabolites associated with Protein digestion and absorption, aminoacyl-tRNA biosynthesis, Biosynthesis of amino acids, Central carbon metabolism in cancer, and ABC transporters. The key metabolites L-Lysine, L-Proline, L-Arginine, and p-Cresol were closely correlated with the differential characteristic bacteria and the characteristic indexes of T2DM. These results suggest that the hypoglycemic effect of the WBMB can be regulated by changes in intestinal flora and metabolites. WBMB can be a functional food with potential for prevention and treatment of T2DM.

Keywords: Whole bitter melon beverage; Type 2 diabetes mellitus; Intestinal flora; Metabolites; Hypoglycemic effect

1. Introduction

T2DM is the central disorder of metabolic syndrome. It has emerged as one of the most prevalent chronic conditions globally, following cancer, and cardiovascular diseases (Dayoub et al., 2015). The incidence of T2DM continues to rise annually due to factors such as poor dietary habits, disrupted lifestyle patterns, and environment degradation. Presently, an estimated 537 million adults worldwide are affected by T2DM, with projections indicating a surge to rise to 783 million by 2045 (Hossain et al., 2024; Shaw et al., 2010), thereby posing a substantial public health concern. Insulin resistance (IR) stands as the primary etiology of T2DM, leading to diminished cellular sensitivity to insulin at standard concentrations. Consequently, despite ongoing insulin production, cellular resistance ensues. Prolonged hyperglycemia can trigger a cascade of

***Corresponding author**
chen-jun1986@hotmail.com

Received 29 July 2025
Received in revised from 11 September 2025
Accepted 6 March 2026

complications, including diabetic cardiovascular diseases, nephropathy, retinopathy, and neuropathy (Lu et al., 2024; Mugisha et al., 2016). Therefore, diabetes and its associated complications significantly jeopardize human health, diminish patient's quality of life, and impose substantial economic burdens on both society and families.

Currently, the treatment for T2DM mainly includes sulfonylureas, thiazolidinediones, glucagon-like peptide-1 receptor agonists, sodium-glucose cotransporter-2 inhibitors, and dipeptidyl peptidase inhibitors. These medications not only help reduce glycated hemoglobin levels but also eliminate the need for subcutaneous injections in patients (Abid et al., 2016; Kalathiya et al., 2025). However, the potential effects of these synthetic drugs on cardiovascular diseases, pancreatitis, and other conditions remain unclear, and patients may experience side effects such as upper respiratory tract infections, nasopharyngitis, and headaches (Mundal et al., 2016). Therefore, there is a pressing necessity to develop green, safe, and effective natural bioactive compounds for the targeted intervention of T2DM. Botanical therapy has become an important strategy for the prevention and control of chronic and infectious diseases in global medical practice (Marrone et al., 2025). According to World Health Organization statistics, approximately 80% of the global population relies on plant-based medicines as primary healthcare, which is closely associated with their phytochemical constituents abundantly present in agricultural by-products. Bitter melon (*Momordica charantia* L.) is rich in a variety of nutrients and exerts multiple pharmacological effects, including hypoglycemic, antitumor, antioxidant, antibacterial, and antiviral activities, as well as immunomodulatory properties. Among these, its modulating effect on T2DM has attracted widespread attention.

Bitter melon and its extracts demonstrate remarkable blood glucose-regulating effects through multi-target mechanisms, with active components acting on multiple key pathways of glucose metabolism. Studies have shown that the intake of bitter melon juice has a regulatory effect on T2DM rats by reducing fasting blood glucose (FBG) and insulin levels, improving blood lipids and oxidative stress, enhancing β-cell function, and alleviating pancreatic islet tissue damage (Mahmoud et al., 2017). Additionally, after three months of bitter melon intervention, T2DM patients exhibited significant reductions in FBG, body weight, and body fat percentage, along with a marked improvement in insulin secretion (Cortez-Navarrete et al., 2018). It has been reported that the hypoglycemic effect of bitter melon is related to its saponins (Atlas, 2015), peptides (Micha et al., 2017), and polysaccharides (Kim et al., 2020; Liu et al., 2021). However, current commercial bitter melon beverages undergo filtration processing that removes dietary fiber and various phytochemicals, leading to significant nutrient loss. There is therefore an urgent need to develop unfiltered bitter melon beverages to maximally preserve their complete nutritional profile.

In this study, the high-energy medium mill (HEMM) independently developed by our research team was used to prepare whole bitter melon pulp (WBMP), and the optimal parameters were optimized by characterizing the changes of functional activity of WBMP under different grinding time. Then, the widely-targeted metabolomics analysis of WBMP under this parameter was carried out, and the key targets were predicted and verified by network pharmacology and molecular docking. Finally, the hypoglycemic

function and potential molecular mechanism of this WBMB were evaluated by establishing T2DM mice model.

2. Materials and methods

2.1 Materials and Reagents

Bitter melon was purchased from Jiangda South Road Farmers' Market, Qingshanhu District, Nanchang City, Jiangxi Province. Ginsenoside standard, glucose standard, 2,2‘-diphenyl-1-picrylhydrazylphenylhydrazyl (DPPH), 2,2’-biazobis-3-ethylbenzothiazoline-6-sulfonic acid (ABTS), α-glucosidase (A3176, enzyme activity ≥5 U/mg), acarbose, PBS buffer, and p-nitrophenyl-β-D-galactopyranoside (pNPG) were purchased from Sigma-Aldrich Corporation (St. Louis, MO,USA). Streptozotocin (USP grade) and metformin hydrochloride (purity≥98.0%) were purchased from Yuanye Biotechnology Co. Ltd. (Shanghai, China). Glucose (analytically pure) was provided by Solebo Technology Co. Ltd. (Beijing, China). All kits were purchased from Nanjing Jiancheng Bioengineering Institute (Nanjing, Jiangsu Province, China). The antibodies ACTIN, SRC, STAT3, P-STAT3, AKT1, P-AKT1, PIK3CA, and PIK3R1 were all purchased from Servicebio Biotechnology Co., Ltd.

2.2 Preparation of whole bitter melon pulp and WBMB

WBMP was prepared by HEMM after preliminary pulverization (3 times) in a colloid mill for different grinding times (30, 60, 90, and 120 min), and the untreated pulp was used as the control group (0 min) (Fig. 1). The WBMP was stored at 4 °C for later experimental determination. According to the results of the functional activity evaluation experiments, the WBMP under 120 min treatment condition was screened for phytochemical substance determination and freeze-drying treatment, and the freeze-dried samples were used to formulate different concentrations of WBMB for animal experiments.

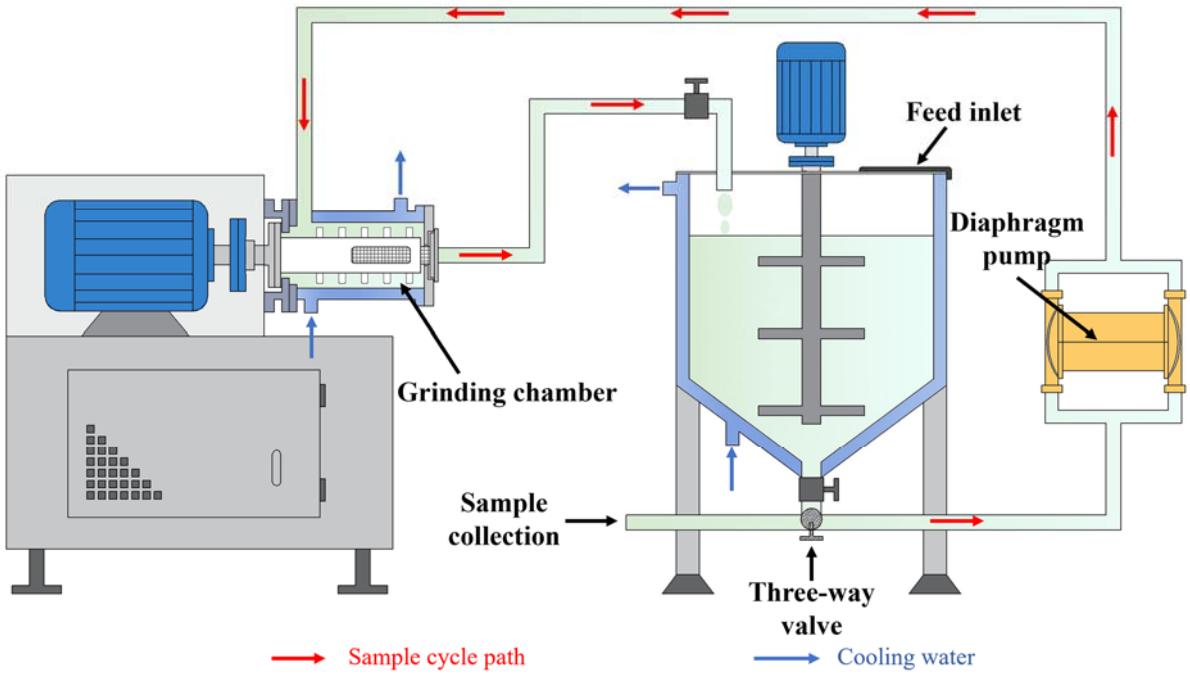

Fig. 1. Structure diagram of the HEMM.

2.3 Determination of the content of active ingredients

2.3.1 Determination of crude saponin content

A volume of 125 mL of 75% anhydrous ethanol was added to 15 g of WBMP, followed by reflux extraction at 70 °C for 2 h. After cooling, the suspension was vacuum-filtered and the filtrate concentrated at 60 °C. The concentrate was re-dissolved in 80 % (v/v) distilled water and partitioned twice against 30 mL of petroleum ether; the combined organic layers were reduced to 40 mL. The resulting concentrate was then extracted three times with 30 mL of saturated n-butanol. The pooled butanolic phase was evaporated under reduced pressure to yield a brown viscous residue, which was taken up in methanol and adjusted to a defined volume in a volumetric flask to furnish the test solution. For quantification, 0.05 mL of the test solution was assayed spectrophotometrically; the crude saponin content in bitter melon was calculated using

$$w=(m_1\times V_1)/(M_1\times V_2),$$

where $\mathbf{m_1}$ denotes the saponin mass (mg) in the test solution determined from the calibration curve, $\mathbf{V_1}$ is the final dilution volume (mL), $\mathbf{m_2}$ is the sample mass (g), and $\mathbf{V_2}$ is the volume (mL) used for colorimetric analysis.

2.3.2 Determination of crude polysaccharide content

Water-dispersed WBMP was extracted at 90 °C (1:1 w/v) for 2 h with constant agitation; the process was duplicated and the resulting supernatants pooled. Absolute ethanol was then added to reach a final concentration of 80 % (v/v) and the mixture was equilibrated at 4 °C overnight. The alcohol-induced precipitate was collected by centrifugation (4 000 rpm, 10 min), rinsed twice with anhydrous ethanol, and dried at 50 °C. The dried polysaccharide was fully solubilised in hot water with stirring, brought to 200 mL, and its content quantified by the phenol–sulfuric acid assay. An aliquot (0.4 mL) of the polysaccharide solution was transferred to a test tube, treated successively with 1 mL of 5 % (w/w) phenol and 5 mL of concentrated H_2SO_4, and left at ambient temperature for 10 min. After incubation at 40 °C for 15 min, the absorbance was read at 490 nm. The crude polysaccharide yield in bitter-melon whole pulp, expressed as milligrams glucose equivalent per gram dry weight, was computed as

$$w=(m_1\times V_1)/(m_2\times V_2)\ \times 0.9\times 10^{-1},$$

where $\mathbf{m_1}$ is the glucose equivalent (μg) from the calibration curve, $\mathbf{V_1}$ is the total extract volume (mL), $\mathbf{m_2}$ is the sample mass (g), and $\mathbf{V_2}$ is the volume (mL) subjected to colorimetry; **0.9** corrects free glucose to anhydrous glucan.

2.4 Antioxidant activity assay

Antioxidant capacity was evaluated by the DPPH• and ABTS•+ assays following the protocol of Zhang et al. (2024) with minor modifications. Freeze-dried WBMP (0.5 g) was suspended in 10 mL anhydrous methanol and sonicated for 30 min. After centrifugation (8000 rpm, 10 min, 4 °C), the clear supernatant was retained for subsequent analyses.

2.4.1 DPPH free radical scavenging rate

A 0.5 mL aliquot of the methanolic extract was combined with 3.0 mL of 0.2 mM DPPH solution. After vigorous mixing, the mixture was incubated in darkness at ambient temperature for 30 min, and the absorbance was recorded at 517 nm. The scavenging activity (%) was calculated as

DPPH free radical scavenging activity $=[1-(A_1-A_2)/A_0]\times100$,

where $\mathbf{A_0}$ is the absorbance of the DPPH solution without extract, $\mathbf{A_1}$ is the absorbance of the extract with DPPH, and $\mathbf{A_2}$ is the absorbance of the extract without DPPH.

2.4.2 ABTS free radical scavenging rate

An aliquot of 150 mL of the sample extract was combined with 3.0 mL of pre-formed ABTS• solution (0.2 mM). After equilibration for 30 min in darkness at ambient temperature, the absorbance was measured at 734 nm. The scavenging capacity (%) was computed as

ABTS free radical scavenging activity $=[A_b-A_s/A_b]\times100$,

where $\mathbf{A_b}$ and $\mathbf{A_s}$ denoting the absorbances of the control and test solutions, respectively..

2.5 Determination of hypoglycemic activity in vitro

Following Ni et al. (2020) with minor adjustments, α-glucosidase (10 mg) was solubilised in 100 mL of 0.02 M phosphate buffer (pH 6.8) to obtain a 1 U mL^{-1} stock solution, which was stored for subsequent use. In a 48-well plate, 40 μL of sample, acarbose or buffer was combined with 80 μL of the enzyme solution and pre-incubated at 37 °C for 15 min. The reaction was initiated by adding 80 μL of 2.5 mM p-nitrophenyl-α-D-glucopyranoside. After a further 15 min at 37 °C, the reaction was quenched with 320 μL of 1 M Na_2CO_3, and the absorbance was read at 405 nm. Inhibitory activity (%) was calculated as

hypoglycemic activity$=[1-A_1/A_0]\times100$,

where A_0 and A_1 represent the absorbances of the control and test wells, respectively.

2.6 LC-MS/MS

Following vacuum freeze-drying, 50 mg of sample was extracted with 1 mL of methanol/acetonitrile/water (1:2:1, v/v/v). After 30 s vortexing, steel beads were added and the mixture was milled at 45 Hz for 10 min, then sonicated on ice for 10 min. A 60-min equilibration at −20 °C preceded centrifugation (12 000 rpm, 15 min, 4 °C). The supernatant (300 μL) was filtered through a 0.22 μm membrane, and an aliquot (10 μL) from each vial was pooled to create a QC sample. Chromatography was performed on an Acquity UPLC HSS T3 column (2.1 × 100 mm, 1.8 μm, Waters) at 35 °C. Mobile phase A consisted of 0.1 % formic acid plus 5 mM ammonium acetate in water; mobile phase B was 0.1 % formic acid in acetonitrile. Injection volume was 4 μL and flow rate 350 μL min^{-1}. The gradient was: 0–0.5 min, 2 % B; 0.5–5 min, 50 % B; 5–10 min, 98 % B; 10–14 min, 2 % B.

2.7 Network Pharmacology

The compounds were uploaded to PubChem database (https://pubchem.ncbi.nih.nlm.nih.gov) to retrieve their chemical structures and imported into Swiss ADME platform for screening of active ingredients. The molecular targets were predicted by Swiss Target Prediction database (https://www.Swisstargetprediction.ch),

and the target was set as “homo sapiens”. Targets with a “probability > 0” should be filtered out. All targets were de-emphasized and then the target genes were normalized using the Uniprot database (https://www.uniprot.org) to finally obtain drug-related targets. The GeneCards database (https://www.genecards.org/), OMIM database (https://omim.org/), and TTD database (https://db.idrblab.net/) were used to search for "type 2 diabetes" as the keyword. The retrieved disease targets were then filtered and imported into the Venny platform alongside the drug component targets to identify common targets. The “drug-disease” intersection targets were imported into String database (https://cn.string-db.org/) to obtain the PPI network diagram of the intersection targets, and the network was analyzed by Network Analyzer tool. The network was analyzed using Cytoscape 3.10.2 software to filter the key core points based on the node degree value and construct a key target PPI network diagram.

2.8 Molecular docking

The SDF format files of the 2D structures of the first 5 screened key active ingredients were downloaded using the PubChem database and converted to 3D structures by ChemBio 3D software. Proteins were downloaded from the PDB database. AutoDock Tools 1.5.7 software was used to process target proteins and key active ingredients. Finally, PyMOL software was used to visualize small molecule ligands and protein receptors with low binding energies.

2.9 Mice model of T2DM

Fifty healthy male C57/6J mice were adaptively fed for 7 d and then randomly stratified into a blank control group (n = 10) fed standard chow and a modelling cohort given high-fat diet. After 4 weeks, animals fasted for 12 h received intraperitoneal streptozotocin (40 mg/kg) on three consecutive days while continuing the high-fat regimen. Mice exhibiting fasting blood glucose ≥ 11.1 mmol/L on two successive readings were deemed diabetic and randomly reassigned to five groups (n = 10): (i) low-dose WBMB (BL, 200 mg/kg/d), (ii) high-dose WBMB (BH, 800 mg/kg/d), (iii) metformin positive control (MET) (100 mg/kg/d) (Zhao et al., 2024). The model control group (DC) and blank control group (NC) were given saline by gavage for a period of 4 weeks. All animal experiments were approved by the Institutional Animal Care and Use Committee (IACUC) of Nanchang University (Approval No. NCULAE-20221030039) and were performed in accordance with the NIH Guide for the Care and Use of Laboratory Animals.

2.10 Determination of body weight, food intake, water intake, fasting blood glucose and oral glucose tolerance

Body mass, food and water consumption were recorded daily at a fixed time. Fasting blood glucose (FBG) was determined on days 0, 7, 14, 21 and 28. After the final overnight fast (12 h), mice received 2 g/kg glucose by gavage; tail-vein glucose was measured at 0, 30, 60, 90 and 120 min to calculate the area under the curve (AUC).

2.11 Determination of serum lipid levels and inflammatory factors

Serum concentrations of insulin levels, total triglycerides (TG), total cholesterol (TC), low-density lipoprotein cholesterol (LDL-C), high-density lipoprotein cholesterol (HDL-C), tumour necrosis factor alpha (TNF-α), and interleukin 1beta (1L-1β) were determined using the kit.

2.12 Determination of liver function indicators

Liver homogenates were analysed for alanine aminotransferase (ALT), aspartate aminotransferase (AST), superoxide dismutase (SOD), catalase (CAT), and malondialdehyde (MDA) following the manufacturers' protocols.

2.13 Histopathological sections of the pancreas and liver

For H&E staining, pancreatic and hepatic specimens were fixed in 4 % paraformaldehyde, dehydrated through graded ethanol, embedded in paraffin, sectioned at 5 μm and stained; morphological alterations were examined by light microscopy. For lipid visualization, liver samples were similarly fixed, embedded in OCT, frozen-sectioned (10 μm), stained with Oil Red O and imaged.

2.14 RT-qPCR

Total RNA from liver was extracted and quantified; only samples with A260/A280 ≥ 1.8 were used for reverse transcription. cDNA (100 ng) was amplified in a 10 μL reaction on a 96-well plate using the following programme: 95 °C for 30 s; 40 cycles of 95 °C for 15 s, 60 °C for 30 s. Melting-curve acquisition (65–95 °C, 0.5 °C increments) confirmed amplicon specificity. Relative mRNA levels were calculated by the $2^{-\Delta\Delta Ct}$ method with primers listed in Table 1.

Table 1. Primers used in experiments.

Gene	Sequence 5′-3′
β-GAPDH	FW5′-CCTCGTCCCGTAGACAAAATG-3′ RV5′-TGAGGTCAATGAAGGGGTCGT-3′
SRC	FW5′-AGATCACTAGACGGGAATCAGAGC-3′ RV5′-GCACCTTTTGTGGTCTCACTCTC-3′
STAT3	FW5′-TGCGGAGAAGCATTGTGAGTG-3′ RV5′-TCTTAATTTGTTGGCGGGTCT-3′
AKT1	FW5′-TTTGGGAAGGTGATTCTGGTG-3′ RV5′-CAGGACACGGTTCTCAGTAAGC-3′
PIK3R1	FW5′-TTGACAGTAGGAGGAGGTTGGA-3′ RV5′-CAGGGAGTATTGATCTTCGGTATT3′
PIK3CA	FW5′-TCTCAACTCGCCTCATAGCAG-3′ RV5′-CTTGCTCTGGCACACAGTCAT-3′

2.15 Western Blot

The tissue samples were rinsed with PBS and lysed using a lysis buffer following mechanical homogenization. The total protein supernatant was collected by centrifugation, and its concentration was determined using the BCA assay. Protein samples were denatured in a reducing loading buffer via boiling, followed by separation using SDS-PAGE. The separated proteins were then transferred onto an activated PVDF membrane under constant current conditions. The membrane was blocked with 5% skim milk and subsequently incubated with a specific primary antibody at 4 °C overnight, followed by incubation with an

HRP-conjugated secondary antibody at room temperature for 30 min. After thorough washing with TBST, the signals were visualized using an ECL chemiluminescence substrate and detected with an imaging system.

2.16 Intestinal flora

Fecal DNA was extracted and quality-screened for amplification. Amplicons were pooled, purified, and subjected to end-repair, A-tailing, adapter ligation, and final clean-up to construct sequencing libraries. Raw reads were quality-filtered and trimmed, then denoised by DADA2 (or Deblur) to generate high-resolution amplicon sequence variants (ASVs).

2.17 Metabolomics analysis

Metabolites were separated on a Hypersil Gold C18 column (2.1 × 100 mm, 1.9 μm; 40 °C) using 0.1 % formic acid in water (A) and methanol (B) at 0.2 mL min^{-1}. Gradient: 0–1.5 min, 2 % B; 1.5–3 min, 85 % B; 3–10 min, 100 % B; 10–12 min, 2 % B. MS acquisition was performed in the m/z 100–1500 range.

2.18 Statistical Analysis

Triplicate determinations were performed. Results are presented as mean ± SD and were compared by one-way ANOVA followed by Duncan's post-hoc test (SPSS 25.0). Figures were generated with Origin 2022 and GraphPad Prism 9.0.

3. Results and Discussion

3.1 Analysis of active ingredient content

Bitter melon saponins and polysaccharides are important active ingredients in bitter melon and have various physiological effects such as lowering blood glucose, antioxidant, lowering cholesterol levels, resisting malignant tumours, and enhancing immunity. As shown in Fig. 2, the amount of saponin dissolved in the WBMP increased with the increase of grinding time in the HEMM. Saponin dissolution increased significantly to 6.69 mg/g (an increase of 19.04%) when the grinding time was 120 min. The polysaccharide dissolution also increased with the increase in milling time, and the polysaccharide dissolution of the 120 min sample was 40.03% higher than that of 0 min. The increase in the amount of saponins and polysaccharides dissolved from bitter melon might be attributed to the fragmentation of the bitter melon cell wall under the action of the motion shear, extrusion, and friction forces of the HEMM, which promoted the release of intracellular saponins and polysaccharides from the bitter melon, while the high-molecular polysaccharides might be degraded into the low-molecular ones that had better solubility (Sun et al., 2025).

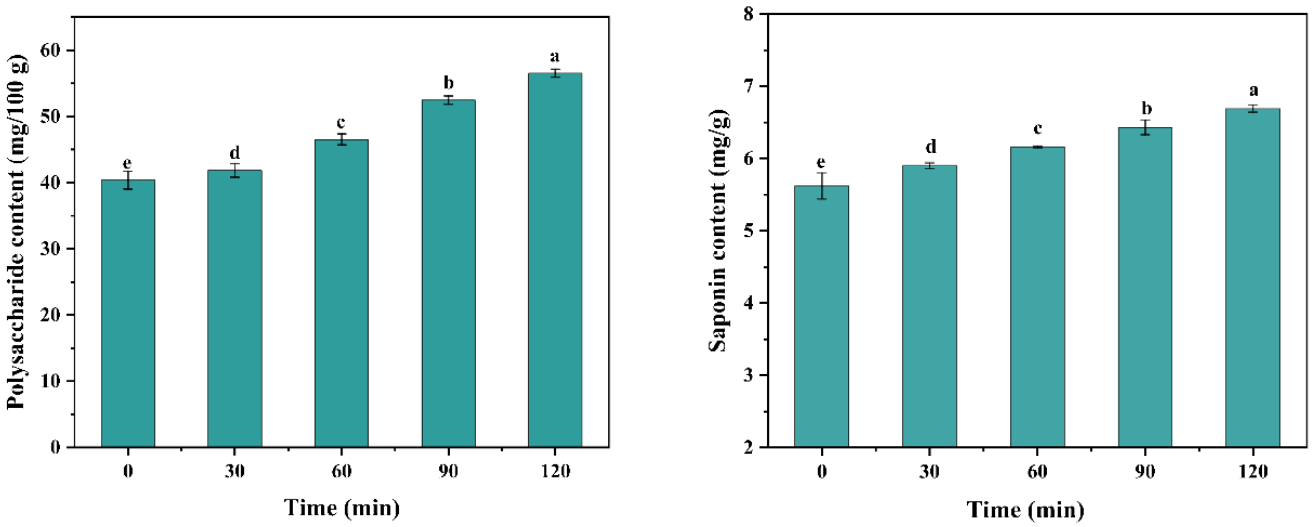

Fig. 2. Effect of HEMM treatment on the contents of saponins and polysaccharides in WBMB.

3.2 Evaluation of antioxidant and hypoglycemic activities

The antioxidant capacity of WBMP was increased after treatment with HEMM, and both DPPH and ABTS radical scavenging reached the highest values at milling up to 90 min, which were 59.39% and 86.24%, respectively (Fig. 3). The increase in antioxidant activity might be attributed to the cell and tissue disruption caused by HEMM, which promoted the release of bioactive compounds with antioxidant properties, such as polyphenols and saponins. The results of Sauceda-Gálvez et al. (2021) also showed that the antioxidant properties of apple juice after ultramicrocrushing were significantly higher compared to untreated juice.

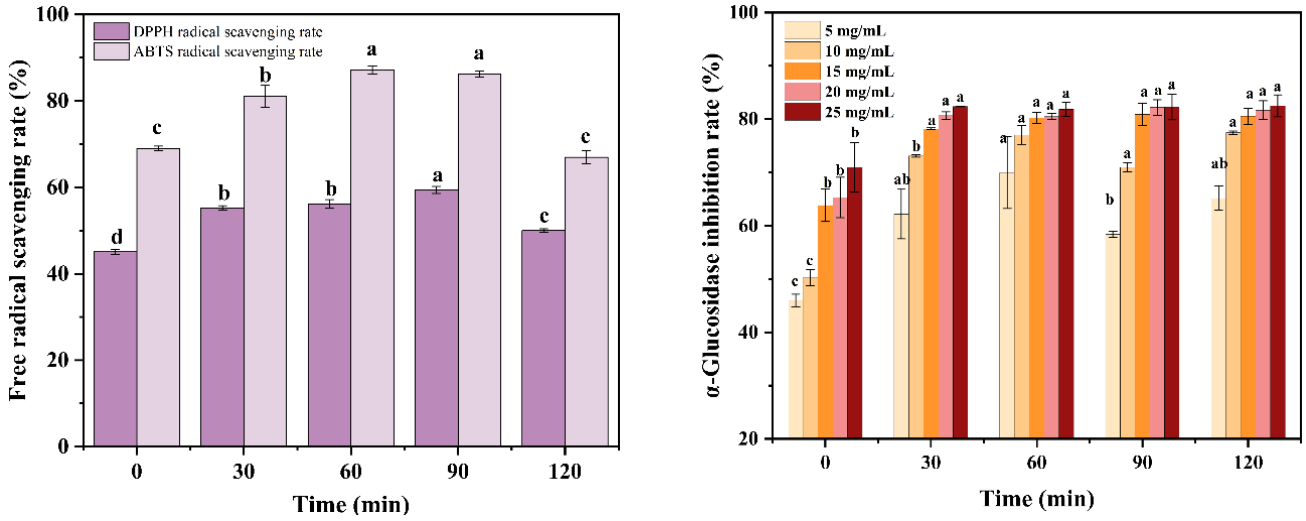

Fig. 3. Effect of HEMM treatment on the *in vitro* antioxidant activity and hypoglycemic activity of WBMB.

Inhibition of α-glucosidase activity can effectively regulate postprandial blood glucose levels in patients with T2DM (Hao et al., 2019; Zheng et al., 2020). As shown in Fig. 3, WBMP inhibited α-glucosidase activity in a dose-dependent manner. Among them, the inhibition of α-glucosidase activity of WBMP after 30 min of grinding by HEMM was significantly enhanced compared with that at 0 min, but there was no significant difference between the samples with different grinding times, and the inhibition rate of α-glucosidase by WBMP could reach 85.86% at the highest. Based on the above experimental results, the WBMP with a

grinding time of 120 min was selected for widely-targeted metabolomics analysis, and WBMB of different concentrations were prepared for animal experiments.

3.3 Network Pharmacology Analysis

A total of 3631 phytochemicals in WBMP were detected using widely-targeted metabolomics, and a total of 37 active ingredients were obtained according to the screening method in section 2.7. The SwissTargetPrediction database yielded 37 unique active-ingredient targets. After duplicate removal, 890 principal gene targets remained. Disease-associated targets for T2DM were retrieved from GeneCards, OMIM and TTD; integration and deduplication produced 1 678 targets. Venn analysis revealed 275 overlapping genes (Fig. 4A). The intersection set was imported into STRING to construct a protein–protein interaction (PPI) network, which was subsequently visualised in Cytoscape 3.10.1. Node centrality was ranked with the cytoNCA plug-in, identifying the top five hub targets. according to the Degree values from the largest to the smallest (Fig. 4B), which were SRC, STAT3, AKT1, PIK3R1, PIK3CA, respectively.

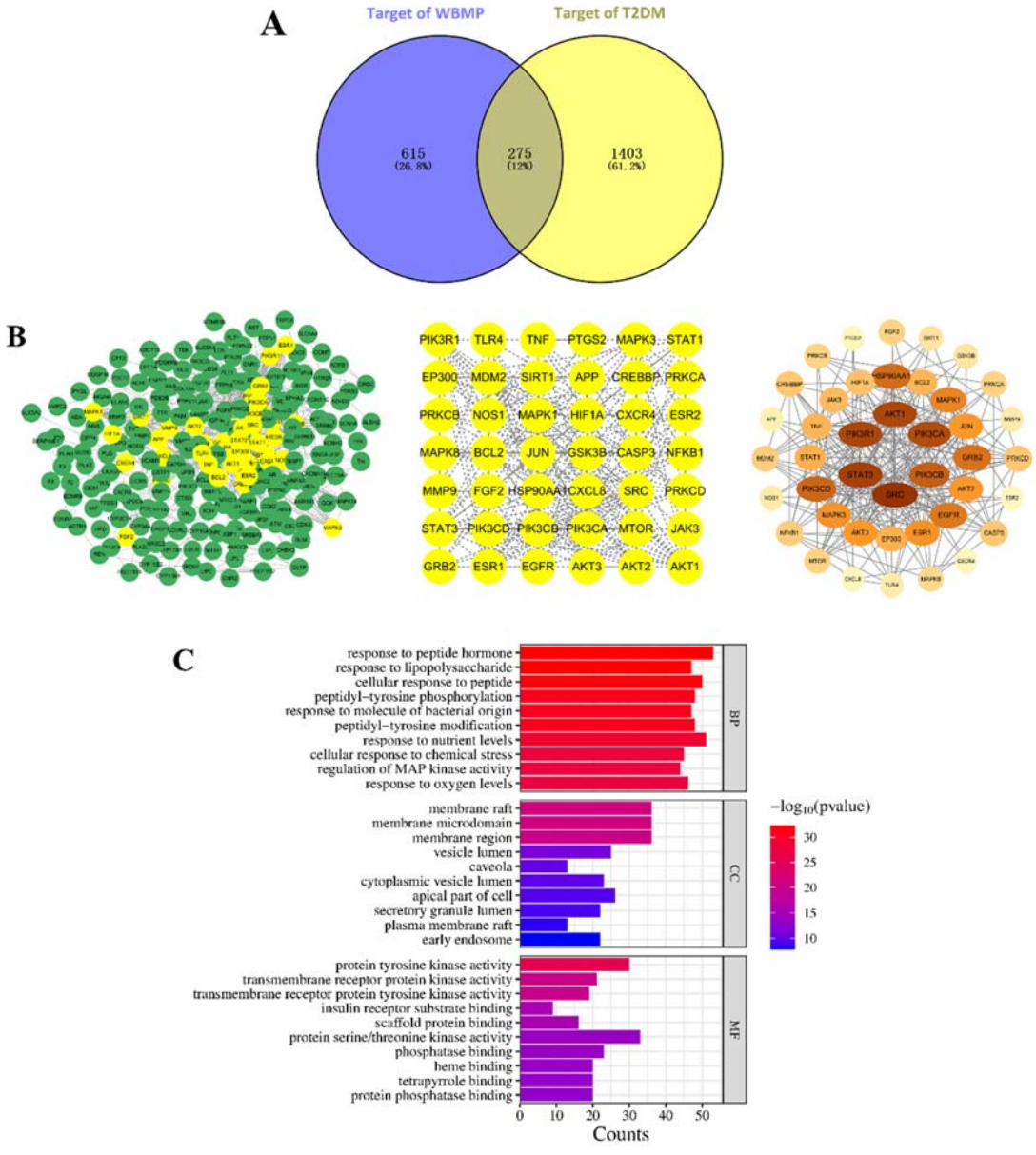

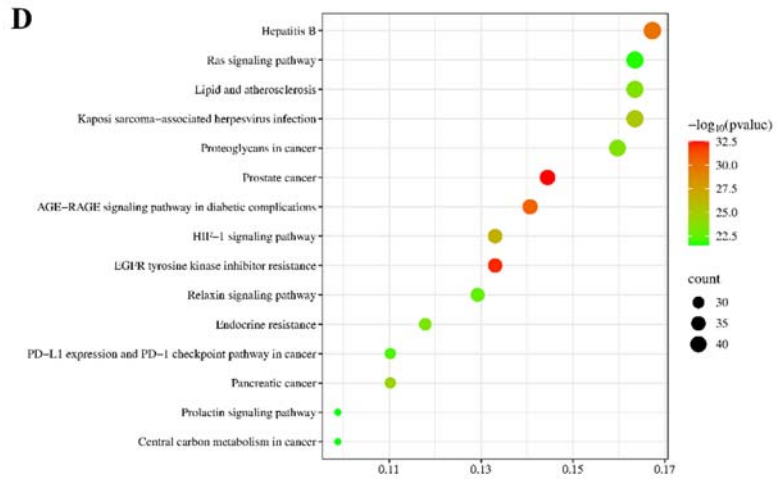

Fig. 4. Network pharmacology Venn diagrams (A) and PPI diagrams (B).

To elucidate the biological effects and potential mechanisms of the active components in WBMP on T2DM, an enrichment analysis was conducted on the potential targets of WBMP for the treatment of T2DM. The results of the GO enrichment analysis were shown in Fig. 4C. Among them, the biological processes (BP) in GO primarily included response to peptide hormone, response to lipopolysaccharide, and cellular response to peptide; The cellular components (CC) included membrane raft, membrane microdomain, and membrane region; The molecular functions (MF) included protein tyrosine kinase activity, transmembrane receptor protein kinase activity, and transmembrane receptor protein tyrosine kinase activity. The KEGG pathway analysis revealed that the significantly enriched signaling pathways for the targets were primarily EGFR tyrosine kinase inhibitor resistance and the AGE-RAGE signaling pathway in diabetic complications (Fig. 4D). Persistent hyperglycemia promoted the formation of Advanced Glycation End-products (AGEs). The binding of AGEs to their receptor (RAGE) activated multiple signaling pathways, including MAPK/ERK, TGF-β, JNK, and NF-κB. This activation led to enhanced oxidative stress and exacerbated inflammatory responses, which subsequently impaired insulin signaling and disrupted metabolic homeostasis. Additionally, it was found to potentially induce cytotoxicity in pancreatic β-cells, thereby contributing to the progression of type 2 diabetes mellitus (Snelson et al., 2022).

3.4 Molecular docking

The three most target-rich constituents of WBMP—Dihydroartemisinin, Crebanine, and Alisol—together with the five highest-degree hubs (SRC, STAT3, AKT1, PIK3R1 and PIK3CA) were selected for docking. Lower binding energies denote stronger, more stable ligand–receptor interactions. In addition, the formation of hydrogen bonds will reduce the free energy of the system, thereby facilitating the binding of ligands to receptors. Therefore, the binding energy and the number of hydrogen bonds are usually important contributors in the scoring function of molecular docking. As shown in Table 2, all three active constituents exhibited binding energies below –5 kcal mol^{-1}, indicative of robust affinity. The most stable complexes were selected for visual inspection in PyMOL, which showed that three hydrogen bonds could be formed between SRC and Alisol via amino acid residues ARG-156, ARG-160, ASN-397 (Fig. 5A), and four hydrogen bonds could be formed between STAT3 and Alisol via amino acid residues GLY-449, LSY- 282,

GLV-448, GLN-361 (Fig. 5B), and 3 hydrogen bonds could be formed between STAT3 and Crebanine via amino acid residues GLN-361, TYR-446, GLU-357 (Fig. 5C). All of the above ligand compounds were well encapsulated in the active pocket of receptor target proteins. The results suggested that SRC, STAT3, AKT1, PIK3R1, and PIK3CA may be potential targets for adjuvant hypoglycemia.

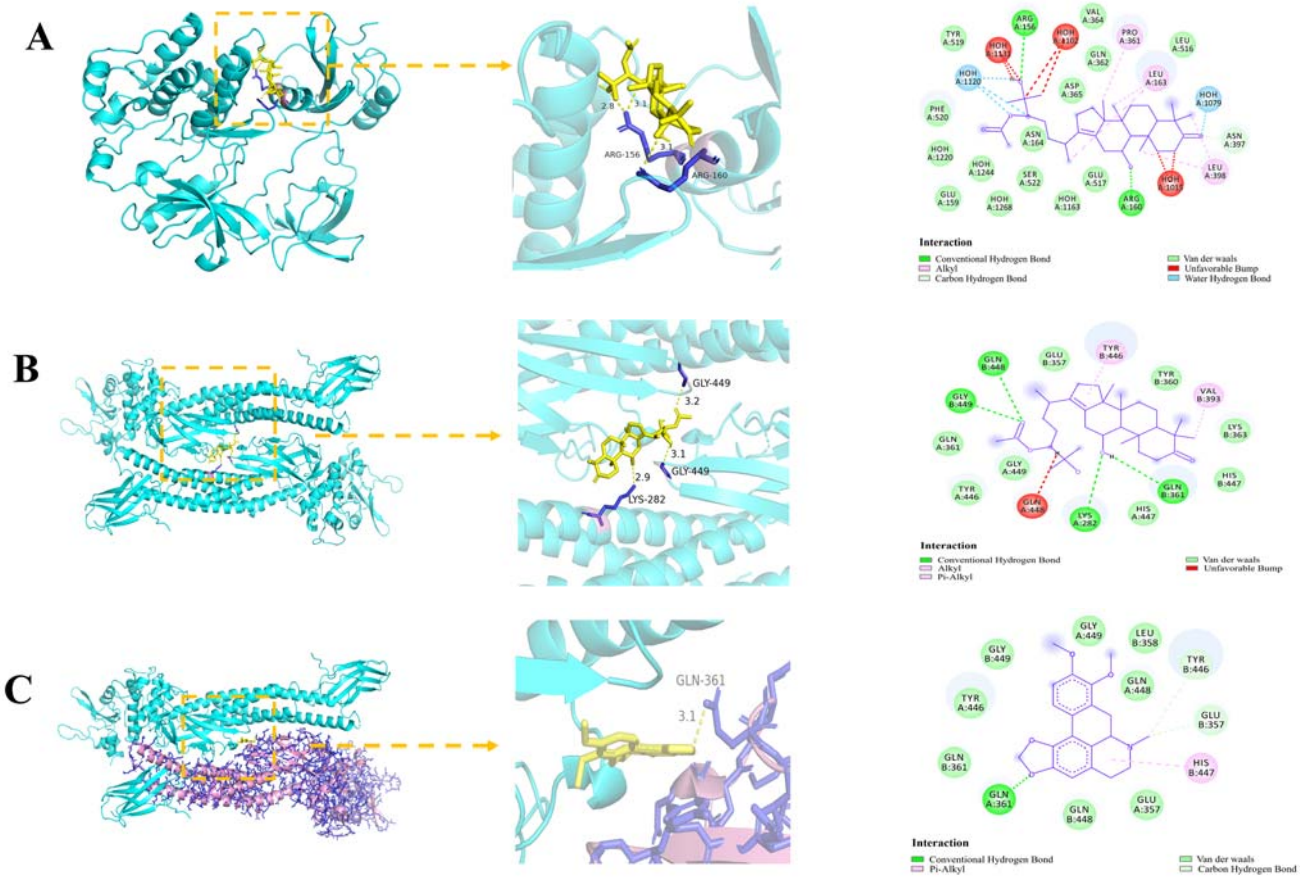

Fig. 5. Molecular docking and visualization of key targets.

Table 2. The free energy of key targets and compounds.

	Targets				
Compounds	SRC	STAT3	AKT1	PIK3R1	PIK3CA
Dihydroartemisinin	-7.5	-7.9	-7.5	-5.9	-8.1
Crebanine	-7.9	-8.3	-7.4	-6.3	-7.1
Alisol	-8.7	-8.2	-8.1	-6.7	-7.5
Estrone	-6.8	-7.2	-7.0	-6.8	-7.9
Camptothecin	-7.3	-7.4	-6.7	-6.9	-7.4

3.5 Effects of different doses of WBMB on body weight, food intake, water intake, fasting blood glucose, and oral glucose tolerance

Except for the NC group, all the other groups showed weight loss and characteristics of drinking and eating more, presenting typical diabetic symptoms. At the end of the intervention, the feed intake and water intake of the mice in the MET, BL, and BH groups decreased significantly compared with the DC group, with the best effect in the MET group, and no significant difference between the BL and BH groups (Fig. 6)

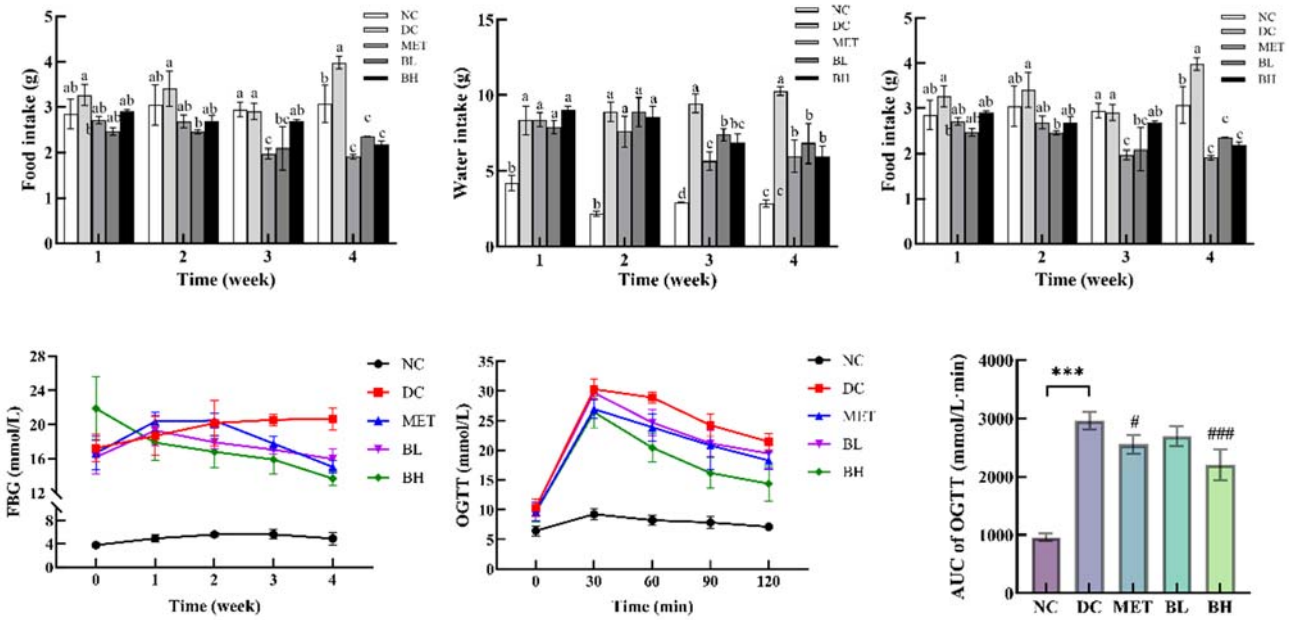

Fig. 6. Effects of WBMB on body weight, food intake, water intake, fasting blood glucose, and oral glucose tolerance. Compared with the NC group, *: $P < 0.05$, **: $P < 0.01$, ***: $P < 0.001$; Compared with the DC group, #: $P < 0.05$, ##: $P < 0.01$, ###: $P < 0.001$, ####: $P < 0.0001$.

Fasting blood glucose is the most commonly used indicator of the body's ability to regulate blood glucose. As seen in Fig. 6, the fasting blood glucose of mice in the NC group was low and stable, while the fasting blood glucose values of mice in the DC group were maintained at a high level throughout the experimental period. The fasting blood glucose values in the MET, BL and BH groups began to decrease after the intervention, among which the decrease in the BH group was the greatest. It indicated that WBMB improved blood glucose regulation ability of diabetic mice. The hypoglycemic effect was comparable to that of the positive control substance metformin hydrochloride and showed dose dependence. WBMB elicited a dose-dependent hypoglycaemic response in diabetic mice comparable to metformin. During oral glucose tolerance test (OGTT), blood glucose peaked at 30 min in all groups before declining. Throughout the test, diabetic mice exhibited higher levels than non-diabetic controls. Moreover, BL, BH and MET groups displayed markedly lower peaks than the DC group. AUC analysis revealed no significant change in the BL group, whereas BH group significantly reduced AUC relative to DC group, indicating that high-dose WBMB improves glucose tolerance and metabolic regulation in T2DM mice.

3.6 Serum insulin, blood lipid, liver function, oxidative stress, and inflammatory factor levels

Serum insulin in the DC group was markedly elevated versus NC group; WBMB intervention dose-dependently restored insulin to baseline, indicating effective suppression of compensatory hyperinsulinaemia. The imbalance of lipid metabolic homeostasis, as a typical complication of diabetes mellitus, is significantly pathologically associated with disorders of glucose metabolism, therefore, regulating lipid metabolism can help to improve diabetes mellitus (Eid et al., 2019). In T2DM mice, serum TG, TC, and LDL-C were elevated and HDL-C was reduced relative to non-diabetic controls. Administration of WBMB or

metformin reversed these anomalies in a dose-dependent manner, demonstrating that WBMB effectively ameliorates T2DM-associated dyslipidaemia.

ALT and AST, key liver aminotransferases, are primarily located in hepatocytes. Their serum levels rise during hepatic damage, making them important clinical indicators of liver function (Peng et al., 2019). Compared with non-diabetic controls, mice of DC group exhibited markedly elevated hepatic ALT and AST activities, whereas MET, BL, and BH treated animals showed significant reductions, indicating that WBMB effectively mitigates T2DM-induced hepatocellular injury. The results indicated that WBMB could attenuate diabetes-induced liver injury and protect liver tissues in mice with dose-dependent effect. The oxidative stress generated by the hyperglycemic state deteriorates the antioxidant defense mechanism of the organism, which leads to elevated MDA content and reduced activity of antioxidant enzymes such as SOD and CAT (Adachi et al., 1996). Hepatic MDA was elevated and SOD and CAT activities were suppressed in DC group, whereas MET, BL, and BH treatments restored antioxidant enzyme activity and reduced lipid peroxidation, confirming that WBMB alleviates T2DM-associated hepatic oxidative stress. Chronic inflammation occurs in diabetic patients. TNF-α and IL-1β are inflammatory factors secreted by inflammatory cells (Jang et al., 2021). Serum TNF-α and IL-1β were markedly elevated in DC group relative to NC group. Four-week WBMB administration dose-dependently reduced both cytokines, demonstrating its capacity to mitigate T2DM-induced systemic inflammation (Fig. 7).

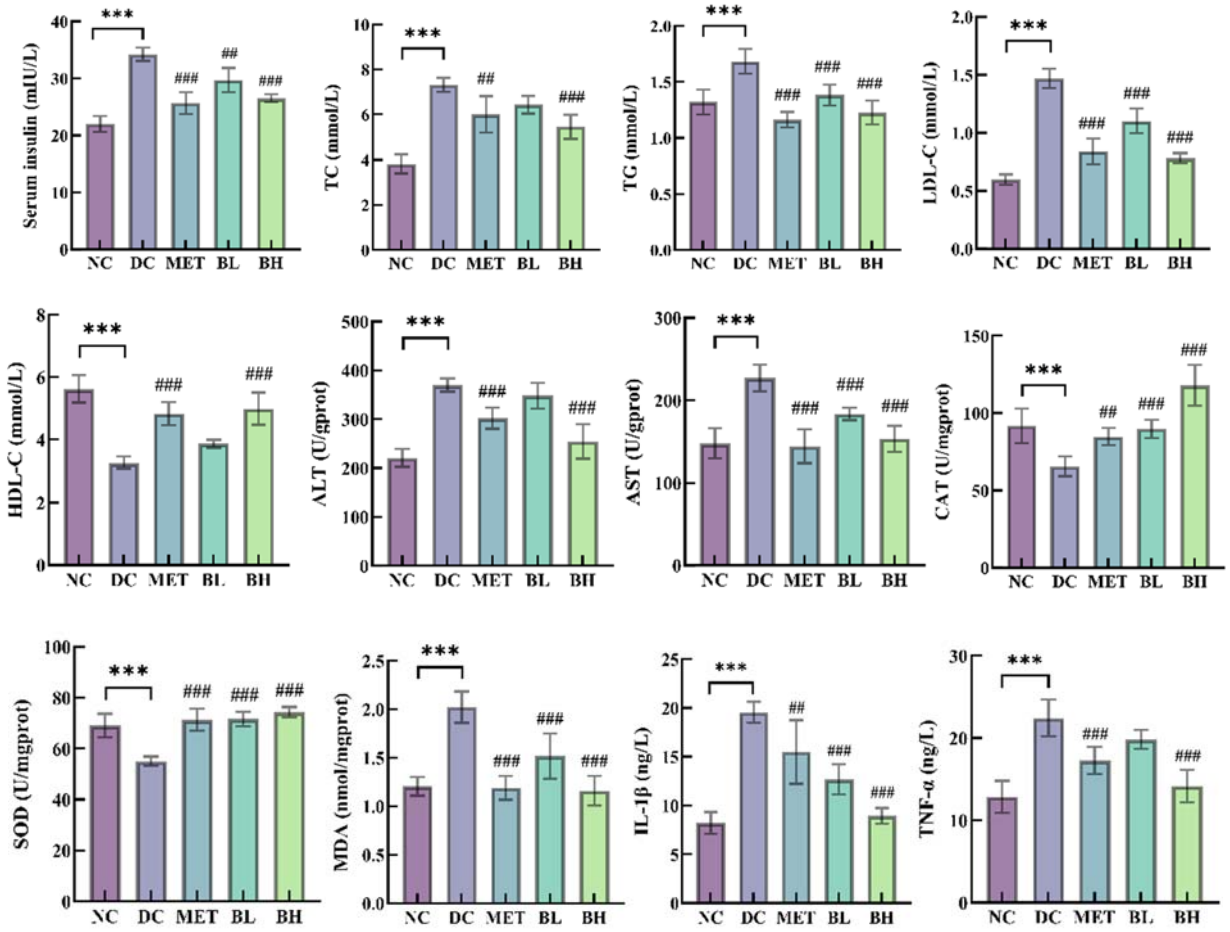

Fig. 7. Effects of WBMB on serum insulin, blood lipid, liver function, oxidative stress, and inflammatory factor levels. Compared with the NC group, *: $P < 0.05$, **: $P < 0.01$, ***: $P < 0.001$; Compared with the DC group, #: $P < 0.05$, ##: $P < 0.01$, ###: $P < 0.001$, ####: $P < 0.0001$.

3.7 Histopathological analysis of pancreatic and liver tissues

The pathological morphology of the pancreas of mice in each group was shown in Fig. 8A. The pancreas of mice in the NC group had a normal morphology, with intact islet structure, large β-cells, and tightly arranged. Compared with the NC group, the pancreatic islets in the DC group had an abnormal morphology, irregular shape, β-cell atrophy, and reduced cell volume and density. This was due to the toxicity of STZ to pancreatic islet β-cells, which can lead to dysfunction of pancreatic islet β-cells and morphological abnormalities (Oliyaei et al., 2021). Compared with the DC group, the MET, BL, and BH groups all showed that the morphology of pancreatic islets was repaired, and the size, number, and arrangement orderliness of β-cells were significantly improved, and the effect of the BH group was the most significant. These results indicated that WBMB had a protective effect on pancreatic islet β-cells.

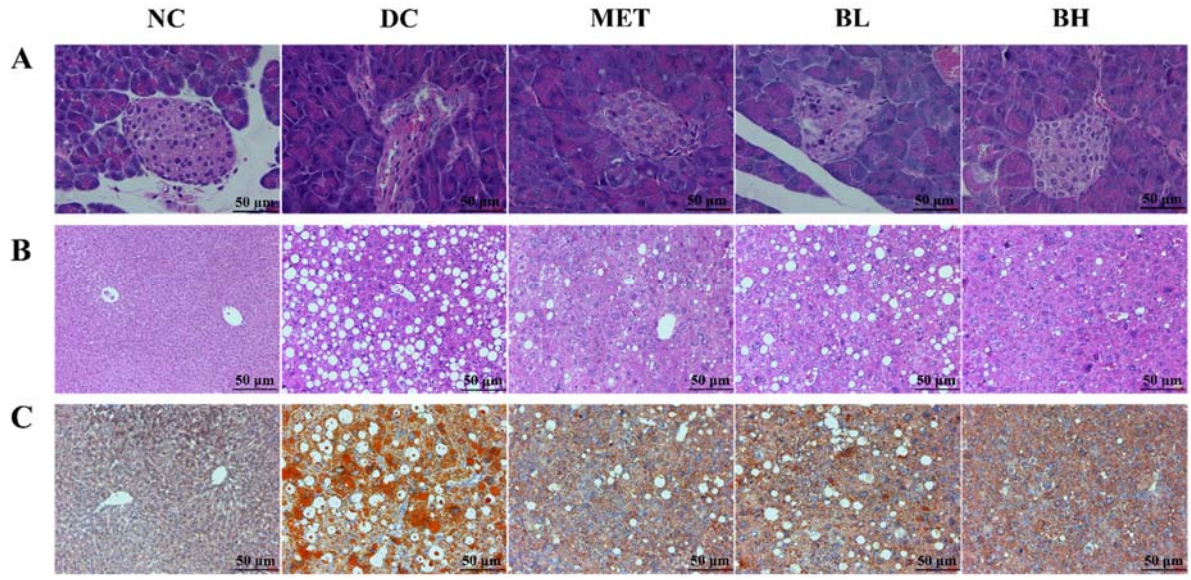

Fig. 8. Pathological sections of the pancreas (A) and liver (B, C).

The results of liver H&E staining sections were shown in Fig. 8B, where the hepatocytes of mice in the NC group were arranged in a single radial row centered on the central vein, and the morphology of the hepatocytes was uniform. In contrast, mice in the DC group showed an abnormal increase in hepatocyte size accompanied by structural disorder, disappearance of intercellular boundaries, and widely distributed lipid vacuole infiltration. Compared with the DC group, this pathological feature was alleviated to varying degrees in the MET, BL, and BH groups. The irregular fat vacuoles decreased, and the cellular interstitial spaces gradually became clear. Among them, the BH group demonstrated the most significant hypoglycemic effect. The characteristics of liver lipid accumulation in the oil red O staining results showed consistency with the previous findings. As shown in Fig. 8C, a large number of fat vacuoles and red lipid droplets were seen in the pictures of the DC group. The MET, BL, and BH groups showed varying degrees of reduction in these lipid deposits, with corresponding attenuation of fat accumulation. Notably, the BH group exhibited the most pronounced improvement. The above results suggested that WBMB could alleviate diabetes-induced liver injury by reducing fat accumulation in liver cells.

3.8 Analysis of key targets

Studies have shown that insulin resistance is one of the central mechanisms in the pathogenesis of T2DM. SRC, a non-receptor tyrosine kinase, can exacerbate insulin resistance by inhibiting insulin signaling through modulating the phosphatidylinositol 3-kinase/protein kinase B (PI3K/AKT) signaling (Ye et al., 2025). STAT3 is a key transcription factor in the JAK-STAT signaling pathway, which is involved in the signaling of multiple cytokines and hormones. In T2DM, abnormal activation of STAT3 may lead to disturbances in the insulin signaling pathway and affect the normal action of insulin (Harada et al., 2023). AKT1 is a key protein in the insulin signaling pathway involved in the regulation of glucose uptake and metabolism. In T2DM, reduced activity of AKT1 may lead to impaired insulin signaling, thereby exacerbating insulin resistance (Gaudreau-Rousseau et al., 2023). Study has found that mice lacking one allele of the PIK3CA gene exhibited glucose intolerance and hyperinsulinemia, indicating that PIK3CA plays a critical role in maintaining glucose homeostasis (Terayama et al., 2025). PIK3R1 regulates insulin signaling by binding to insulin receptor substrate (IRS). Abnormal function of PIK3R1 may lead to interruption or disruption of the insulin signaling pathway, which in turn triggers insulin resistance (Huang et al., 2018). The top 5 targets SRC, STAT3, AKT1, PIK3CA, and PIK3R1 were screened by network pharmacology. Therefore, RT-qPCR quantitative analysis was performed on the liver of mice with T2DM, and it was found that the expression levels of SRC, STAT3, and PIK3R1 were down-regulated after high-dose of WBMB intervention. The expression levels of AKT1 and PIK3CA were upregulated, but there was no significant difference between the low-dose WBMB beverage group and the DC group (Fig. 9A). It was indicated that high-dose of WBMB could prevent the occurrence and development of T2DM by down-regulating SRC, STAT3, and PIK3R1 and up-regulating the expression of the AKT1. The expression levels of these five potential target proteins, as well as phosphorylated STAT3 and phosphorylated AKT1 proteins, were also consistent with the results obtained by qPCR. (Fig. 9B).

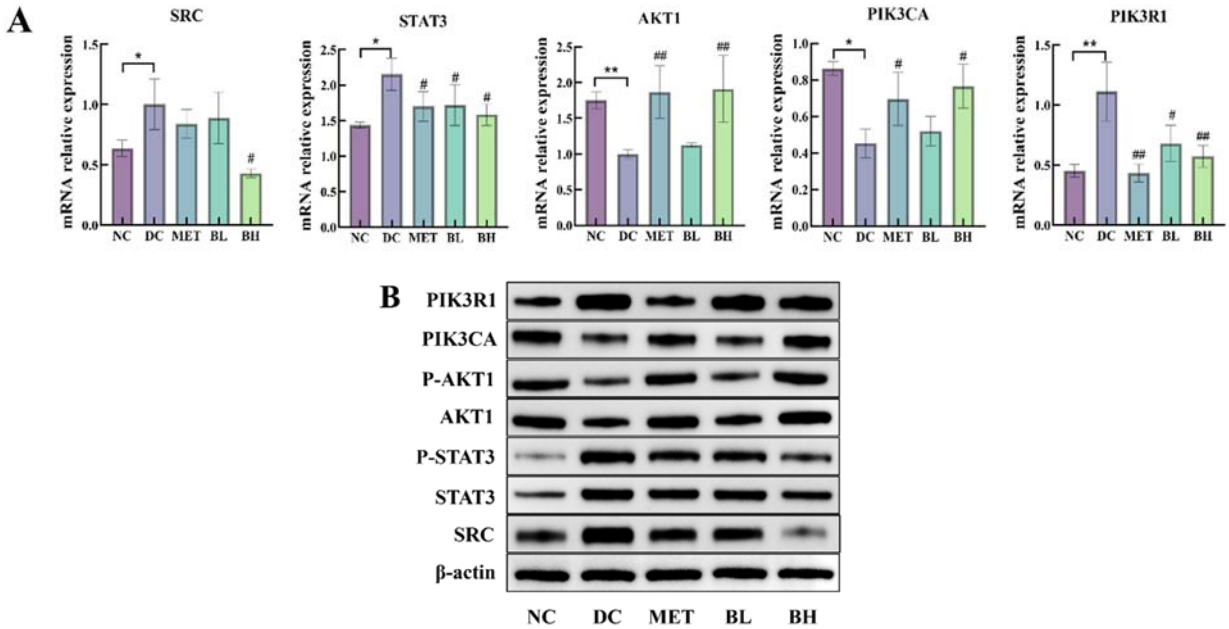

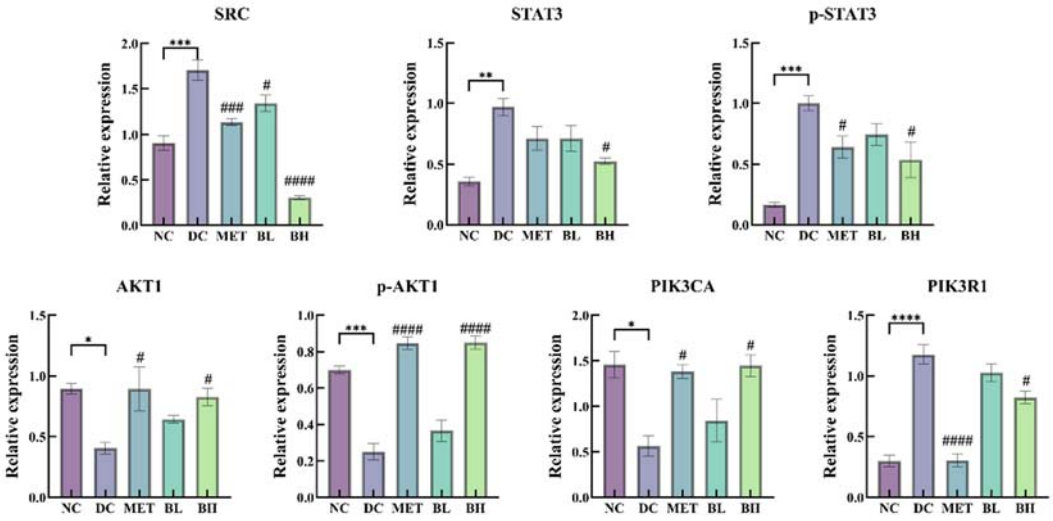

Fig. 9. The relative expression levels of key target genes (A) and proteins (B). Compared with the NC group, *: $P < 0.05$, **: $P < 0.01$, ***: $P < 0.001$; Compared with the DC group, #: $P < 0.05$, ##: $P < 0.01$, ###: $P < 0.001$, ####: $P < 0.0001$.

3.9 Analysis of intestinal flora

3.9.1 Alpha and Beta diversity analysis

Alpha diversity is a key indicator of species diversity, reflecting the composition, structure, and function of microbial communities (Willis, 2019). The diversity of microbial communities in each group of mice was evaluated by comparing the Shannon and Simpson indices of their intestinal flora communities. Fig. 10A showed the Shannon and Simpson indices of each group. The Shannon and Simpson indices revealed that DC group exhibited significantly reduced gut microbial diversity compared with NC group, whereas BH treatment restored these indices to levels comparable with NC group, indicating that high-dose WBMB partially reinstated intestinal microbial richness in T2DM mice.

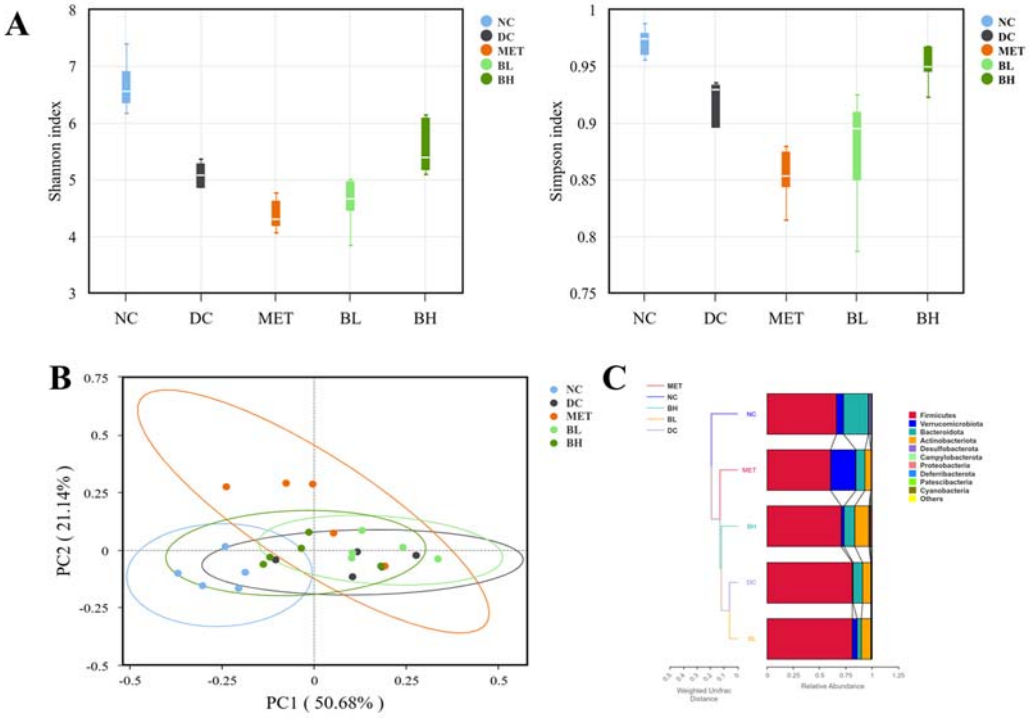

Fig. 10. Analysis of α-diversity (A) and β-diversity (B, C) of intestinal flora.

Beta diversity analysis is an analytical method commonly used to compare diversity between ecosystems and differences between samples, and includes a variety of analytical methods such as PCoA analysis and UPGMA analysis (Andermann et al., 2022). According to the results of PCoA, it can be seen that the samples of the DC group had a large difference compared with the NC group, while the samples of the BH group and the NC group had an increased intersection, indicating that the high dose of WBMB could improve the structure of the intestinal flora of the diabetic mice to a certain extent (Fig. 10B). According to the results of UPGMA, it can be seen that the species composition of the DC group was significantly different from that of the NC group and the samples were farther away from each other, whereas the samples of the MET and BH groups were closer to the samples of the NC group, which suggested that the WBMB could change the species composition of microorganisms in T2DM mice (Fig. 10C).

3.9.2 Analysis of microbiota composition

At the phylum level, *Firmicutes*, *Verrucomicrobia*, and *Bacteroidetes* predominated. Relative to NC group, DC group exhibited elevated Firmicutes and reduced Bacteroidetes; MET, BL, and BH treatments reversed these shifts, restoring proportions comparable to controls. Among them, the MET group exhibited the most pronounced changes, followed by the BH group (Fig. 11A). Studies had shown that *Bacteroidetes* abundance was decreased and *Firmicutes* abundance was increased in diabetic mice. These microbial alterations might contribute to T2DM pathogenesis by modulating intestinal barrier function and energy metabolism (Ding et al., 2019; Yuan et al., 2019; Zhao et al., 2017). At the genus level, *Dubosiella* and *Akkermansia* were the dominant genera (Fig. 11B). *Dubosiella* belongs to *Firmicutes*, a genus of intestinal flora newly identified in recent years, and preliminary study had shown that its elevated abundance might be a compensatory response of the intestinal flora in the early stages of metabolic imbalance that was associated with diabetes and metabolic disorders (Li et al., 2024). *Akkermansia* improves glycaemic control and insulin sensitivity while restraining pro-inflammatory cytokines, and its depletion correlates with obesity, T2DM and inflammatory bowel disease, highlighting its probiotic potential (Iatcu et al., 2021). As can be seen from Fig. 11C, compared with NC group, DC group exhibited reduced *Akkermansia* and elevated *Dubosiella*, a dysbiotic signature that was reversed by WBMB intervention. These dysbiotic patterns were effectively reversed by MET, BL, and BH group, as evidenced by significantly reduced *Dubosiella* levels and elevated *Akkermansia* levels when compared to the DC group. Notably, the BH group was observed to significantly increase the abundance of *Bifidobacterium*—a well-established probiotic genus scientifically validated to regulate gut microbiota homeostasis, enhance intestinal barrier function, and modulate metabolic processes. (Alessandri et al., 2021; Ewaschuk et al., 2008). The above results suggested that WBMB might improve glucose metabolism and strengthen the intestinal barrier by up-regulating the abundance of *Bacteroidetes*, *Akkermansia*, *Bifidobacterium* and down-regulating *Dubosiella* to alleviate T2DM.

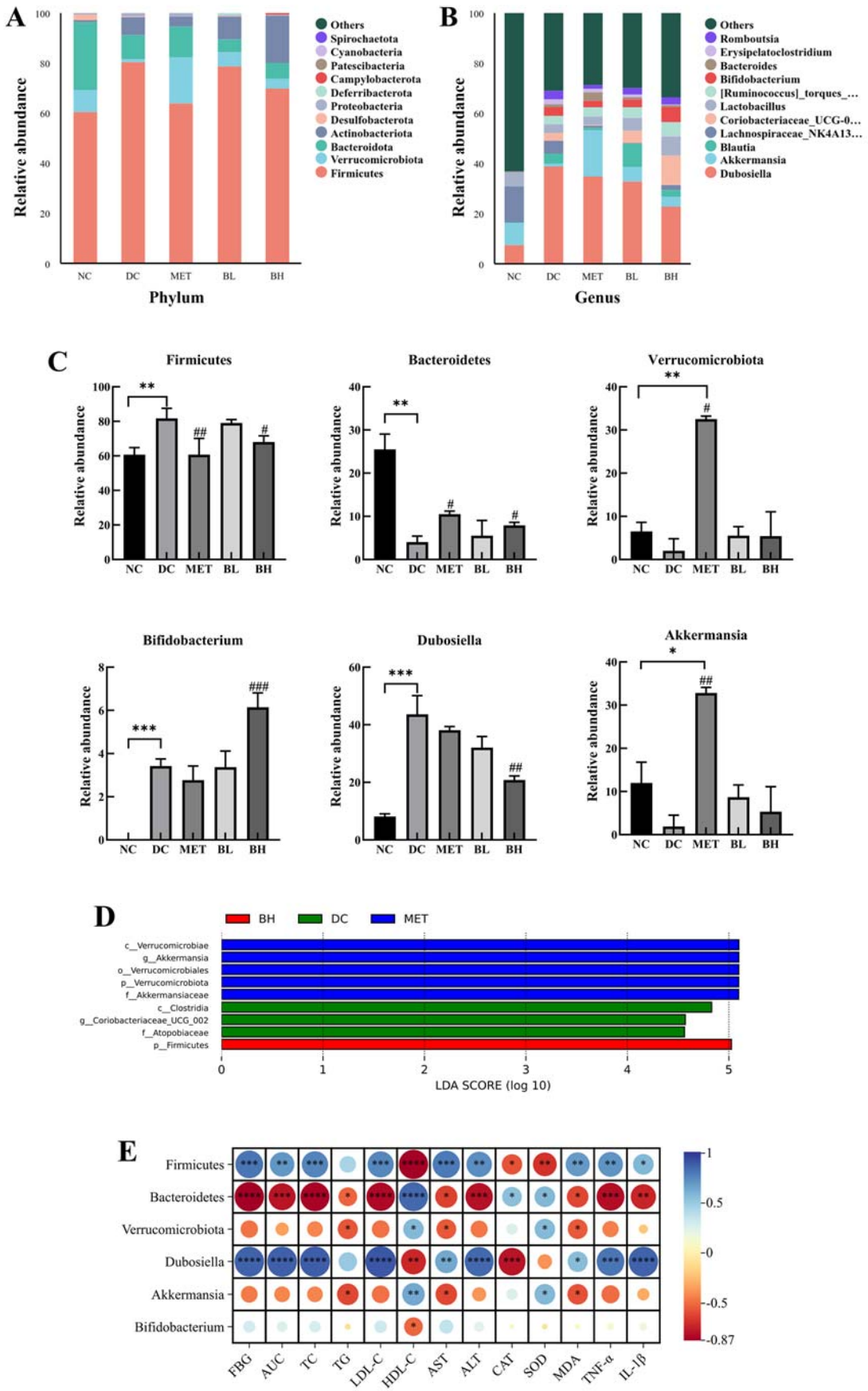

Fig. 11. The relative abundance of intestinal flora at the phylum level (A) and genus level (B) and analysis of differential species (C), LEfSe (D), and correlation of characteristic flora with characteristic indicators of T2DM (E). Compared with the NC group, *: $P < 0.05$, **: $P < 0.01$, ***: $P < 0.001$; Compared with the DC group, #: $P < 0.05$, ##: $P < 0.01$, ###: $P < 0.001$, ####: $P < 0.0001$.

LEfSe analysis is mainly used to identify microbial taxa (phyla, genera, strains) that are significantly different between different groups, and its core objective is to screen for biomarkers that are closely related to specific biological conditions (Gao et al., 2022). As shown in Fig. 11D, the differential species in the intestinal flora of the DC group were mainly *Clostridia*, *Coriobacteriaceae*_UCG_002, and *Atopobiaceae*, suggesting that the above species might be the key biomarkers leading to the development of T2DM. In the MET group, differential species included Verrucomicrobiota, Verrucomicrobiae, Verrucomicrobiales, Akkermansia, and Akkermansiaceae, while the BH group was characterized by Firmicutes, indicating that these taxa may serve as biomarkers for glucose-lowering effects. In order to investigate the correlation between intestinal flora and T2DM characteristics after the intervention of WBMB, Spearman's rank correlation analysis was used to determine the relationship between differential phyla and genera and metabolic characteristics of T2DM. As shown in Fig. 11E, significant correlations were presented between the different phyla and genera and most of the T2DM metabolic profiles, suggesting that the WBMB could regulate the host metabolic processes in mice through the intestinal flora, thus exerting a hypoglycemic effect.

3.10 Metabolomics analysis

A non-parametric test of the DC/NC, BL/DC, and BL/DC groups showed that there were 720 differential metabolites in the DC/NC group, of which 254 differential metabolites were up-regulated and 466 differential metabolites were down-regulated, and the top 5 metabolites that were significantly changed were 1-Palmitoyl-sn-glycero-3-phosphocholine, 16:0 LYSO-PE, 3-(3-sulfooxyphenyl)propanoic Acid, β-Tocotrienol, and sequirin B. There were 54 differential metabolites in the BL/DC group, of which 22 differential metabolites were up-regulated and 32 differential metabolites were down-regulated, and the top 5 most significant changes were 4-Carboxypyrazole, Central carbon metabolism in cancerBeesioside D, N-Octanoyl-L- homoserine lactone, Docosatrienoic Acid, and Pandangolide 4. There were 64 differential metabolites in the BH/DC group, of which 37 differential metabolites were up-regulated and 27 differential metabolites were down-regulated, and the top 5 differential metabolites were 4,4‘-Diapolycopene, D-Mannosamine, 8’-apo-beta-Carotenol, Ecliptasaponin A, and Isoeleutherin (Fig. 12A, B, C). Venn diagrams were used to demonstrate the differences and overlap of metabolites between the different groups. Comparative analysis demonstrated that high-dose WBMB treatment normalized 17 dysregulated metabolites (both upregulated and downregulated) in the DC group, while low-dose WBMB treatment restored 12 aberrant metabolites. (Fig. 12D).

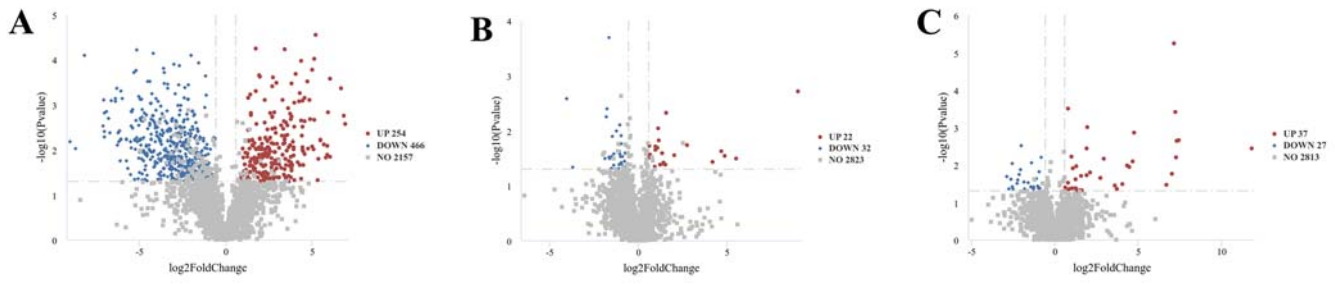

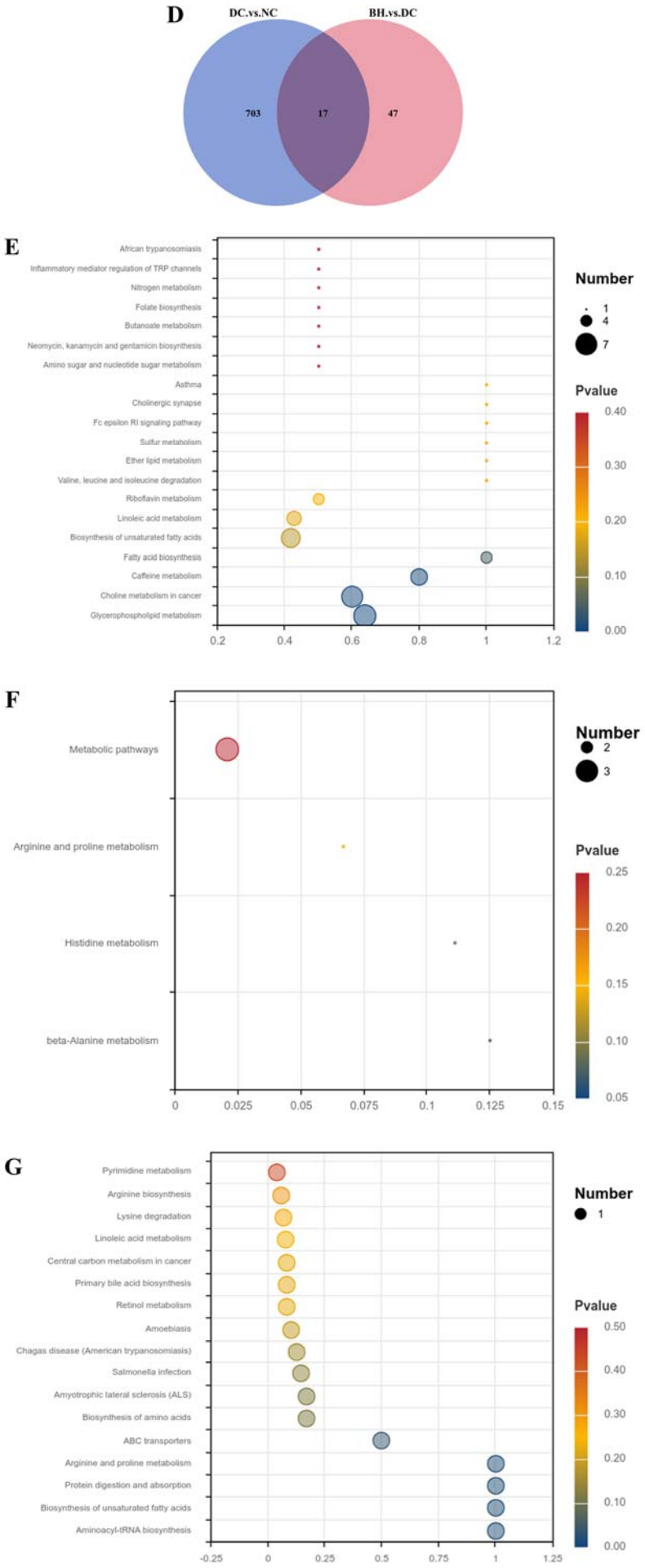
D
DC.vs.NC
BH.vs.DC
703
17
47
E
African trypanosomiasis
Inflammatory mediator regulation of TRP channels
Nitrogen metabolism
Folate biosynthesis
Butanoate metabolism
Neomycin, kanamycin and gentamicin biosynthesis
Amino sugar and nucleotide sugar metabolism
Asthma
Cholinergic synapse
Fc epsilon RI signaling pathway
Sulfur metabolism
Ether lipid metabolism
Valine, leucine and isoleucine degradation
Riboflavin metabolism
Linoleic acid metabolism
Biosynthesis of unsaturated fatty acids
Fatty acid biosynthesis
Caffeine metabolism
Choline metabolism in cancer
Glycerophospholipid metabolism
0.2
0.4
0.6
0.8
1
1.2
Number
1
4
7
Pvalue
0.40
0.30
0.20
0.10
0.00
F
Metabolic pathways
Arginine and proline metabolism
Histidine metabolism
beta-Alanine metabolism
0
0.025
0.05
0.075
0.1
0.125
0.15
Number
2
3
Pvalue
0.25
0.20
0.15
0.10
0.05
G
Pyrimidine metabolism
Arginine biosynthesis
Lysine degradation
Linoleic acid metabolism
Central carbon metabolism in cancer
Primary bile acid biosynthesis
Retinol metabolism
Amoebiasis
Chagas disease (American trypanosomiasis)
Salmonella infection
Amyotrophic lateral sclerosis (ALS)
Biosynthesis of amino acids
ABC transporters
Arginine and proline metabolism
Protein digestion and absorption
Biosynthesis of unsaturated fatty acids
Aminoacyl-tRNA biosynthesis
-0.25
0
0.25
0.5
0.75
1
1.25
Number
1
Pvalue
0.50
0.40
0.30
0.20
0.10
0.00

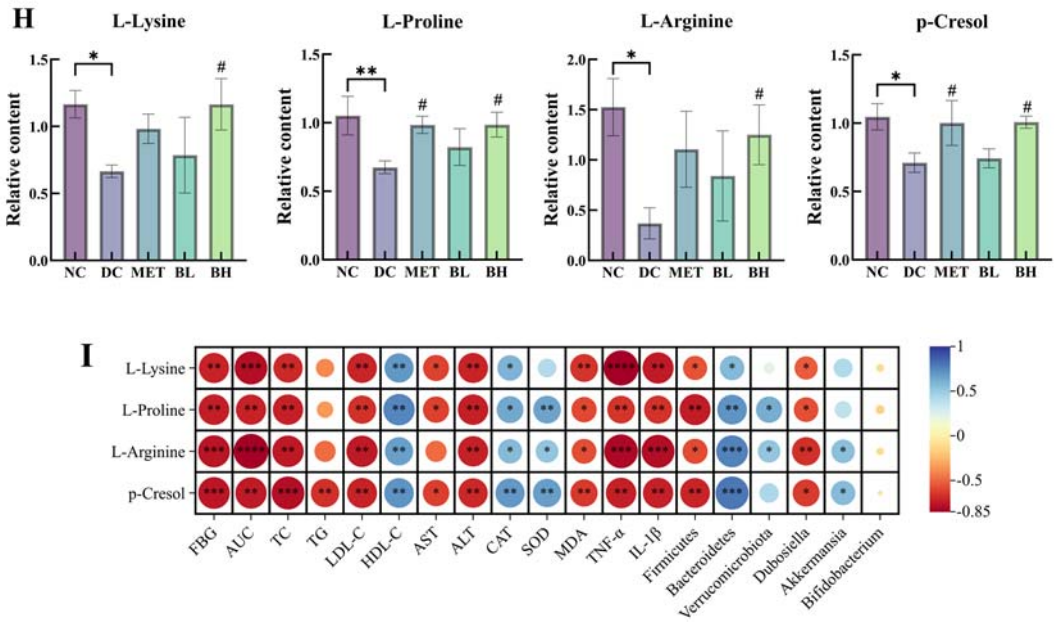

Fig. 12. Volcano diagrams (A, B, C), Venn diagrams (D), KEGG pathway diagrams of serum differential metabolites (E, F, G), relative content diagrams of key differential metabolites (H), and correlation diagrams of key differential metabolites with characteristic indicators and key differential microbiota. Compared with the NC group of T2DM (I), *: $P < 0.05$, **: $P < 0.01$, ***: $P < 0.001$; Compared with the DC group, #: $P < 0.05$, ##: $P < 0.01$, ###: $P < 0.001$, ####: $P < 0.0001$.

Significant changes were observed in 4, 1, and 5 metabolic pathways when the DC group was compared with the NC group, BL group, and BH group, respectively. In the comparison between the DC and NC groups, significant alterations were found in Glycerophospholipid metabolism, Choline metabolism in cancer, Caffeine metabolism, and Fatty acid biosynthesis. Pentose and glucuronate interconversions were significantly altered between BL and DC groups. Protein digestion and absorption, Aminoacyl-tRNA biosynthesis, Biosynthesis of amino acids, Central carbon metabolism in cancer, and ABC transporters were significantly altered between BH and DC groups (Fig. 12E, F, G). Notably, the degree of alteration was more pronounced in the BH group compared to the BL group, in which elevated levels of branched-chain amino acids (BCAAs) in the Protein digestion and absorption pathway were strongly associated with the risk of T2DM, and prolonged high levels of BCAAs may lead to over-activation of the mTOR signaling pathway, which may in turn trigger early β-cell dysfunction and damage (Hao et al., 2023). Aminoacyl-tRNA biosynthesis may play an important role in the development and progression of T2DM, and abnormalities in amino acid metabolism may interfere with insulin signaling through activation of the mTOR signaling pathway, thereby affecting insulin sensitivity and leading to insulin resistance (Tian et al., 2017). Other amino acids in the Biosynthesis of amino acids pathway such as tyrosine and tryptophan, in addition to BCAA, have also been associated with the risk of T2DM. For example, tyrosine may affect glucose homeostasis by influencing the synthesis of dopamine and L-DOPA (Jäger et al., 2020). Abnormalities in central carbon metabolism in cancer have similarities with metabolic disorders in T2DM. Hyperglycemia and insulin resistance may lead to cellular metabolic reprogramming that promotes cancer development and progression. This metabolic reprogramming may also affect insulin signaling pathways and cellular functions (Lai et al., 2020). ABC transporters play an important role in cellular metabolism and are involved in the transport of

various substances. They are considered crucial in the regulation of lipid metabolism and cholesterol levels, and their dysfunction may indirectly contribute to the development of T2DM (Tian et al., 2017).

Further analysis of the differential metabolites on the major enrichment pathways between the DC and BH groups showed that there were four differential metabolites in the Protein digestion and absorption pathway, namely L-Lysine, L-Proline, L-Arginine, and p-Cresol. Aminoacyl-tRNA biosynthesis pathway had 3 differential metabolites, namely L-Lysine, L-Proline, and L-Arginine. Biosynthesis of amino acids pathway had 3 differential metabolites, namely L-Lysine, L-Proline, and L-Arginine. Central carbon metabolism in cancer pathway had 2 differential metabolites, L-Proline and L-Arginine. ABC transporters pathway had 3 differential metabolites, namely L-Lysine, L-Proline, and L-Arginine. Overall, a total of 4 differential metabolites were found among the 5 pathways that changed significantly (Fig. 12H). To further clarify the relationship between metabolites and hyperlipidemia as well as intestinal flora after WBMB intervention, Spearman correlation analysis was conducted. It was found that these four differential metabolites showed significant correlations with most of the T2DM characteristic indicators and differential phyla and genera (Fig. 12I). Based on the above results, it was speculated that *Firmicutes*, *Bacteroidetes*, *Dubosiella*, and *Akkermansia* might play a dual role in the regulation of Protein digestion and absorption, Aminoacyl-tRNA biosynthesis, Biosynthesis of amino acids, Central carbon metabolism in cancer, and ABC transporters pathways, as well as in the improvement of lipid metabolism by the WBMB, thereby inhibiting the increase of blood sugar levels and alleviating the occurrence and development of T2DM.

4. Conclusion

In this study, we investigated the hypoglycemic effect of WBMB on STZ-induced diabetic mice. The WBMB intervention significantly reduced blood glucose, lipid and oxidative stress levels, and decreased systemic inflammation and organ damage. The WBMB might influence differential metabolites (L-Lysine, L-Proline, L-Arginine, and p-Cresol) in key metabolic pathways by regulating intestinal flora, and by down-regulating the expression of SRC, STAT3, and PIK3R1 and up-regulating the expression of AKT1 and PIK3CA, thereby improving lipid metabolism, inhibiting the increase of blood sugar levels, and alleviating the progression of type 2 diabetes. Through the whole chain research of "processing technology innovation-active mechanism analysis-functional efficacy verification", this study has enriched the bitter melon food series, increased the transformation pathway of bitter melon resources, and provided scientific support for the in-depth development of medicinal and food plants, as well as the prevention and control of chronic diseases.

Acknowledgements

The authors are grateful for National Key R&D Program of China (grant number 2024YFD2100605), National Natural Science Foundation of China General Program (grant number 32372379), Key Technologies for Functional Food Production and Industrialization Demonstration (grant number 20232BCD44005), National Natural Science Foundation of China Regional Program (grant number 32160572), Central

Government Guide Local Special Fund Project for Scientific and Technological Development of Jiangxi Province (grant number 20241ZDF02087, 20241ZDF02075, and 20241ZDF02078)

Declarations of interest:

The authors declare that they have no known competing financial interest or personal relationships that could have appeared to influence the work reported in this paper.

Statement

The animal study protocol was approved by Animal Experiment Committee of Nanchang University (NCULAE-20221030039).

References

Abid R., Mahmood R., & Santosh Kumar H.S. (2016). Hypolipidemic and antioxidant effects of ethanol extract of Cassia fistula fruit in hyperlipidemic mice. *Pharmaceutical Biology,* 54(12), 2822-2829.https://doi.org/10.1080/13880209.2016.1185445

Adachi T., Nakashima S., Saji S., Nakamura T., & Nozawa Y. (1996). Mitogen-activated protein kinase activation in hepatocyte growth factor-stimulated rat hepatocytes: Involvement of protein tyrosine kinase and protein kinase C. *Hepatology,* 23(5), 1244-1253.https://doi.org/10.1002/hep.510230545

Alessandri G., van Sinderen D., & Ventura M. (2021). The genus Bifidobacterium: from genomics to functionality of an important component of the mammalian gut microbiota. *Computational and Structural Biotechnology Journal,* 19, 1472-1487.https://doi.org/10.1016/j.csbj.2021.03.006

Andermann T., Antonelli A., Barrett R.L., & Silvestro D. (2022). Estimating alpha, beta, and gamma diversity through deep learning. *Frontiers in Plant Science,* 13, 839407.https://doi.org/10.3389/fpls.2022.839407

Atlas D. (2015). International diabetes federation. *IDF Diabetes Atlas, 7th edn. Brussels, Belgium: International Diabetes Federation,* 33(2).

Cortez-Navarrete M., Martínez-Abundis E., Pérez-Rubio K.G., González-Ortiz M., & Méndez-del Villar M. (2018). Momordica charantia Administration Improves Insulin Secretion in Type 2 Diabetes Mellitus. *Journal of Medicinal Food,* 21(7), 672-677.https://doi.org/10.1089/jmf.2017.0114

Dayoub E., & Jena A.B. (2015). Chronic Disease Prevalence and Healthy Lifestyle Behaviors Among US Health Care Professionals. *Mayo Clinic Proceedings,* 90(12), 1659-1662.https://doi.org/10.1016/j.mayocp.2015.08.002

Ding Q., Zhang B., Zheng W., Chen X., Zhang J., Yan R., Zhang T., Yu L., Dong Y., & Ma B. (2019). Liupao tea extract alleviates diabetes mellitus and modulates gut microbiota in rats induced by streptozotocin and high-fat, high-sugar diet. *Biomedicine & Pharmacotherapy,* 118, 109262.https://doi.org/10.1016/j.biopha.2019.109262

Eid S., Sas K.M., Abcouwer S.F., Feldman E.L., Gardner T.W., Pennathur S., & Fort P.E. (2019). New insights into the mechanisms of diabetic complications: role of lipids and lipid metabolism. *Diabetologia,* 62(9), 1539-1549.https://doi.org/10.1007/s00125-019-4959-1

Ewaschuk J.B., Diaz H., Meddings L., Diederichs B., Dmytrash A., Backer J., Looijer-van Langen M., & Madsen K.L. (2008). Secreted bioactive factors from Bifidobacterium infantis enhance epithelial cell barrier function. *American Journal of Physiology Gastrointestinal and Liver Phhysiology,* 295(5), G1025-G1034.https://doi.org/10.1152/ajpgi.90227.2008

Gao X., Liu D., Gao L., Ouyang Y., Wen Y., Ai C., Chen Y., & Zhao C. (2022). Health benefits of Grifola frondosa polysaccharide on intestinal microbiota in type 2 diabetic mice. *Food Science and Human Wellness,* 11(1), 68-73.https://doi.org/10.1016/j.fshw.2021.07.008

Gaudreau-Rousseau C., Bergeron P., Réale D., & Garant D. (2023). Environmental and individual determinants of burrow-site microhabitat selection, occupancy, and fidelity in eastern chipmunks living in a pulsed-resource ecosystem. *PeerJ,* 11, e15110.https://doi.org/10.7717/peerj.15110

Hao D., Wen X., Liu L., Wang L., Zhou X., Li Y., Zeng X., He G., & Jiang X. (2019). Sanshool improves UVB-induced skin photodamage by targeting JAK2/STAT3-dependent autophagy. *Cell Death & Disease,* 10(1), 19.https://doi.org/10.1038/s41419-018-1261-y

Hao Z., Yao J., Zhao X., Liu R., Chang B., & Shao H. (2023). Preliminary observational study of metabonomics in patients with early and late-onset type 2 diabetes mellitus based on UPLC-Q-TOF/MS. *Scientific Reports,* 13(1), 14579.https://doi.org/10.1038/s41598-023-41883-y

Harada T., Nagai K., Mase K., Tsunoda R., Iseki K., Moriyama T., Tsuruya K., Fujimoto S., Narita I., & Konta T. (2023). Elevated Crude Mortality in Obese Chronic Kidney Disease Patients with Loss of Exercise Habit: A Cohort Study of the Japanese General Population. *Internal Medicine,* 62(15), 2171-2179.https://doi.org/10.2169/internalmedicine.0803-22

Hossain M.J., Al-Mamun M., & Islam M.R. (2024). Diabetes mellitus, the fastest growing global public health concern: Early detection should be focused. *Health Science Reports,* 7(3), e2004.https://doi.org/10.1002/hsr2.2004

Huang X., Liu G., Guo J., & Su Z. (2018). The PI3K/AKT pathway in obesity and type 2 diabetes. *International journal of biological sciences,* 14(11), 1483.https://doi.org/10.7150/ijbs.27173

Iatcu C.O., Steen A., & Covasa M. (2021). Gut microbiota and complications of type-2 diabetes. *Nutrients,* 14(1), 166.https://doi.org/10.3390/nu14010166

Jäger S., Cuadrat R., Wittenbecher C., Floegel A., Hoffmann P., Prehn C., Adamski J., Pischon T., & Schulze M.B. (2020). Mendelian randomization study on amino acid metabolism suggests tyrosine as causal trait for type 2 diabetes. *Nutrients,* 12(12), 3890.https://doi.org/10.3390/nu12123890

Jang S.Y., Choi S.H., Kikkawa D., Lee E.J., & Yoon J.S. (2021). Association of fibroblast growth factor 10 with the fibrotic and inflammatory pathogenesis of Graves' orbitopathy. *PloS one,* 16(8), e0255344.https://doi.org/10.1371/journal.pone.0255344

Kalathiya U.N., Herrin J., Swarna K.S., Deng Y., Polley E.C., Neumiller J.J., Galindo R.J., Umpierrez G.E., Ross J.S., Mickelson M.M., et al. (2025). Comparative Risk of Adverse Pancreatic Events with GLP-1 Receptor Agonists, SGLT2 Inhibitors, DPP4 Inhibitors, and Sulfonylureas among Adults with Type 2 Diabetes at Moderate Cardiovascular Disease Risk. *Endocrine Practice*.https://doi.org/10.1016/j.eprac.2025.09.004

Kim S.K., Jung J., Jung J.H., Yoon N., Kang S.S., Roh G.S., & Hahm J.R. (2020). Hypoglycemic efficacy and safety of Momordica charantia (bitter melon) in patients with type 2 diabetes mellitus. *Complementary Therapies in Medicine,* 52, 102524.https://doi.org/10.1016/j.ctim.2020.102524

Lai M., Liu Y., Ronnett G.V., Wu A., Cox B.J., Dai F.F., Röst H.L., Gunderson E.P., & Wheeler M.B. (2020). Amino acid and lipid metabolism in post-gestational diabetes and progression to type 2 diabetes: A metabolic profiling study. *PLOS Medicine,* 17(5), e1003112.https://doi.org/10.1371/journal.pmed.1003112

Li R., Yang P., LI M., YE Z., & Zhang P. (2024). Amelioration of dextran sulfate sodium-induced ulcerative colitis by fermented Lycium barbarum polysaccharides through modulation of intestinal microecology. *Journal of China Pharmaceutical University,* (6), 236-245

Liu Z., Gong J., Huang W., Lu F., & Dong H. (2021). The Effect of Momordica charantia in the Treatment of Diabetes Mellitus: A Review. *Evidence-Based Complementary and Alternative Medicine,* 2021, 3796265.https://doi.org/10.1155/2021/3796265

Lu X., Xie Q., Pan X., Zhang R., Zhang X., Peng G., Zhang Y., Shen S., & Tong N. (2024). Type 2 diabetes mellitus in adults: pathogenesis, prevention and therapy. *Signal Transduction and Targeted Therapy,* 9(1), 262.https://doi.org/10.1038/s41392-024-01951-9

Mahmoud M.F., Ashry F.E.Z.Z.E., Maraghy N.N.E., & and Fahmy A. (2017). Studies on the antidiabetic activities of Momordica charantia fruit juice in streptozotocin-induced diabetic rats. *Pharmaceutical Biology,* 55(1), 758-765.https://doi.org/10.1080/13880209.2016.1275026

Marrone G., Di Lauro M., Cornali K., Masci C., Vanni G., Vita C., & Noce A. (2025). Sustainability and role of plant-based diets in chronic kidney disease prevention and treatment. *Front Pharmacol,* 16, 1562409.https://doi.org/10.3389/fphar.2025.1562409

Micha R., Peñalvo J.L., Cudhea F., Imamura F., Rehm C.D., & Mozaffarian D. (2017). Association Between Dietary Factors and Mortality From Heart Disease, Stroke, and Type 2 Diabetes in the United States. *JAMA,* 317(9), 912-924.https://doi.org/10.1001/jama.2017.0947

Mugisha J.O., J. S.E., Madeleine R., Monica K., Paul K., Joel N., & and Seeley J. (2016). Chronic disease, risk factors and disability in adults aged 50 and above living with and without HIV: findings from the Wellbeing of Older People Study in Uganda. *Global Health Action,* 9(1), 31098.https://doi.org/10.3402/gha.v9.31098

Mundal L., & Retterstøl K. (2016). A systematic review of current studies in patients with familial hypercholesterolemia by use of national familial hypercholesterolemia registries. *Current Opinion in Lipidology,* 27(4), 388-397.https://doi.org/10.1097/MOL.0000000000000300

Oliyaei N., Moosavi-Nasab M., Tamaddon A.M., & Tanideh N. (2021). Antidiabetic effect of fucoxanthin extracted from Sargassum angustifolium on streptozotocin-nicotinamide-induced type 2 diabetic mice. *Food Science & Nutrition,* 9(7), 3521-3529.https://doi.org/10.1002/fsn3.2301

Peng Y., Gao Y., Zhang X., Zhang C., Wang X., Zhang H., Wang Z., Liu Y., & Zhang H. (2019). Antidiabetic and hepatoprotective activity of the roots of Calanthe fimbriata Franch. *Biomedicine & Pharmacotherapy,* 111, 60-67.https://doi.org/10.1016/j.biopha.2018.12.066

Sauceda-Gálvez J.N., Codina-Torrella I., Martinez-Garcia M., Hernández-Herrero M.M., Gervilla R., & Roig-Sagués A.X. (2021). Combined effects of ultra-high pressure homogenization and short-wave ultraviolet radiation on the properties of cloudy apple juice. *LWT,* 136, 110286.https://doi.org/10.1016/j.lwt.2020.110286

Shaw J.E., Sicree R.A., & Zimmet P.Z. (2010). Global estimates of the prevalence of diabetes for 2010 and 2030. *Diabetes Research and Clinical Practice,* 87(1), 4-14.https://doi.org/10.1016/j.diabres.2009.10.007

Snelson M., Lucut E., & Coughlan M.T. (2022). The Role of AGE-RAGE Signalling as a Modulator of Gut Permeability in Diabetes. *International Journal of Moleculer Science,* 23(3), 1766.https://doi.org/10.3390/ijms23031766

Sun M., Li K., Li X., Li J., Men L., Lu M., Gong X., & Li Z. (2025). Phytochemical properties and antioxidative activities of ginseng superfine powders prepared by wet grinding method with high-pressure homogenization. *Powder Technology,* 451, 120448.https://doi.org/10.1016/j.powtec.2024.120448

Terayama K., Furuzono S., Fer N., Yan W., Young L.C., Czyzyk D.J., et al. (2025). Molecular glues that facilitate RAS binding to PI3Kα promote glucose uptake without insulin. *Science (New York, N.Y.)*, *389*(6758), 402–408. https://doi.org/10.1126/science.adr9097

Tian S., Xu Q., Jiang R., Han T., Sun C., & Na L. (2017). Dietary protein consumption and the risk of type 2 diabetes: a systematic review and meta-analysis of cohort studies. *Nutrients,* 9(9), 982.https://doi.org/10.3390/nu9090982

Willis A.D. (2019). Rarefaction, alpha diversity, and statistics. *Frontiers in microbiology,* 10, 2407.https://doi.org/10.3389/fmicb.2019.02407

Ye C., Li Y., Shi J., He L., Shi X., Yang W., Lei W., Quan S., Lan X., & Liu S. (2025). Network pharmacology analysis revealed the mechanism and active compounds of jiao tai wan in the treatment of type 2 diabetes mellitus via SRC/PI3K/AKT signaling. *Journal of Ethnopharmacology,* 337, 118898.https://doi.org/10.1016/j.jep.2024.118898

Yuan Y., Zheng Y., Zhou J., Geng Y., Zou P., Li Y., & Zhang C. (2019). Polyphenol-Rich Extracts from Brown Macroalgae Lessonia trabeculate Attenuate Hyperglycemia and Modulate Gut Microbiota in High-Fat Diet and Streptozotocin-Induced Diabetic Rats. *Journal of Agricultural and Food Chemistry,* 67(45), 12472-12480.https://doi.org/10.1021/acs.jafc.9b05118

Zhang Y., Yin H.N., Wang A.Y., Zhang Y.H., Guo Z., Ye Y.Y., & Chen M.B. (2024). Bioaccessibility and antioxidant activity of fermented chrysanthemum rice wine on *In vitro* simulated digestion. *Food Bioscience,* 62, 105144.https://doi.org/10.1016/j.fbio.2024.105144

Zhao, D., Luo, Z., Li, S., Liu, S., & Wang, C. (2024). Metabolomics Revealed the Effects of *Momordica charantia* L. Saponins on Diabetic Hyperglycemia and Wound Healing in Mice. *Foods*, 13(19), 3163. https://doi.org/10.3390/foods13193163

Zhao L., Zhang Q., Ma W., Tian F., Shen H., & Zhou M. (2017). A combination of quercetin and resveratrol reduces obesity in high-fat diet-fed rats by modulation of gut microbiota. *Food & Function,* 8(12), 4644-4656.https://doi.org/10.1039/C7FO01383C

Zheng Y., Tian J., Yang W., Chen S., Liu D., Fang H., Zhang H., & Ye X. (2020). Inhibition mechanism of ferulic acid against α-amylase and α-glucosidase. *Food Chemistry,* 317, 126346.https://doi.org/10.1016/j.foodchem.2020.126346